Electronic Supplementary Material (ESI) for RSC Advances.

Supporting Information

for

Zinc Bimetallics Supported by Xanthene-Bridged Dinucleating Ligand: Synthesis, Characterization, and Lactide Polymerization Studies

Thilini S. Hollingsworth,[a] Ryan L. Hollingsworth,[a] Tomer Rosen,[b*] Stanislav Groysman[a*]

[a]Department of Chemistry, Wayne State University, Detroit, Michigan 48202, United States.

[b] School of Chemistry, Raymond and Beverly Sackler Faculty of Exact Sciences, Tel-Aviv University, Tel-Aviv 69978, Israel.

*To whom the correspondence should be addressed. E-mail: tomer.rsn@gmail.com, groysman@chem.wayne.edu

Table of Contents ***page***

1. Crystallographic Information

X-ray Crystallographic Details. The structures of **L** (*syn*-parallel and *anti*-parallel conformers), **1-5**, **7** and **8** were determined by X-ray crystallography. A Bruker APEXII/Kappa three circle goniometer platform diffractometer with an APEX-2 detector was used for data collection. A graphic monochromator was employed for the wavelength selection (Mo Kα radiation, $\lambda = 0.71073$ Å). The data were processed and the structure was solved using the APEX-2 software. The structure was refined by standard difference Fourier techniques with SHELXL (6.10 v., Sheldrick G. M., and Siemens Industrial Automation, 2000). Hydrogen atoms were placed in calculated positions using a standard riding model and refined isotropically; all other atoms were refined anisotropically (except specific cases described below). Structure-specific data collection and refinement information is given in Table S1in the Supporting Information. The structure of L^{syn} contained one solvent molecule per asymmetric unit displaying translational disorder. The solvent was modeled as hexane and ether with partial occupancies. Compound **2** contained one hexane molecule in the asymmetric unit, located on a special position. Compound **3** contained two disordered solvent molecules per asymmetric unit, one of which was modeled as hexane in two alternative conformations, and the other was modeled as ether in three alternative conformations. None of the disordered solvent molecules were refined anisotropically. Compound **4** contained two ^{t}Bu groups displaying large wagging motion. The disorder in these tBu groups was modeled as two alternative conformations of unequal occupancies; the conformation with the larger occupancy was refined anisotropically. Compound **5** contained two ether molecules per asymmetric unit, one of which was found to be disordered over two conformations. In addition, one of the zinc-bound ethyl groups exhibited two alternative conformations. Compound **7** contained one toluene molecule per asymmetric unit, which demonstrated translational disorder.

Due to the disorder, the solvent was not refined anisotropically. In addition, one of the ^{t}Bu groups was disordered over two conformations. In the structure of compound **8**, the complex was located at the special position. Therefore, only half of the complex molecule constituted the asymmetric unit. The structure contained one ether molecule per asymmetric unit.

Table S1. Experimental crystallographic parameters for **L^{syn}**, **L^{anti}**, **1-5**, **7**, and **8**.

	L^{syn}	**L^{anti}**	**1**	**2**	**3**
formula	$C_{53}H_{72}N_2O_3$ ×0.5OEt_2 ×0.5C_6H_{14}	$C_{53}H_{72}N_2O_3$	$C_{34}H_{54}ClLiO_3Zn$	$C_{53}H_{70}N_2O_3Zn$ ×$C_{15}H_{24}O$ ×C_6H_{12}	$C_{61}H_{86}Li_3N_2O$ ×0.5OEt_2 ×1.5C_6H_{14}
Fw, g/mol	891.22	785.13	618.53	1092.84	1092.77
temperature	100(2)	100(2)	100(2)	100(2)	100(2)
cryst syst	triclinic	monoclinic	monoclinic	monoclinic	orthorhombic
space group	*P-1*	*P*2$_1$/n	*P*2$_1$/n	*Cc*	*P*bca
color	yellow	yellow	colorless	yellow	yellow
Z	2	4	4	4	8
a, Å	14.0407(12)	16.5356(7)	9.9180(13)	29.7214(18)	15.7195(9)
b, Å	14.9293(12)	14.7630(6)	25.002(4)	22.1597(18)	28.5190(17)
c, Å	15.0232(12)	19.9092(8)	13.3687(14)	10.3440(6)	30.8537(18)
α, deg	63.972(4)	90.00	90.00	90.00	90.00
β, deg	84.451(4)	103.180(2)	97.840(5)	109.183(4)	90.00
γ, deg	74.293(4)	90.00	90.00	90.00	90.00
V, A^3	2723.2(4)	4732.1(3)	3284.1(7)	6434.5(8)	13831.8(14)
d_{calcd}, g/cm^3	1.087	1.102	1.251	1.128	1.050
μ, mm^{-1}	0.066	0.067	0.860	0.428	0.064
2θ, deg	47.00	55.14	51.68	50.78	48.44
R_1[a] (all data)	0.1548	0.0806	0.0788	0.0662	0.1469
wR_2[b] (all data)	0.2976	0.1974	0.1571	0.1307	0.2421
R_1[a] [(I>2σ)]	0.0951	0.0666	0.0561	0.0472	0.0887
wR_2[b] [(I>2σ)]	0.2848	0.1853	0.1491	0.1219	0.2111
GOF (F^2)	1.001	1.028	1.072	1.018	1.064

[a] $R_1 = \Sigma||F_o| - |F_c||/\Sigma|F_o|$. [b] $wR_2 = (\Sigma(w(F_o^2 - F_c^2)^2)/\Sigma(w(F_o^2)^2))^{1/2}$. [c] GOF = $(\Sigma\ w(F_o^2 - F_c^2)^2/(n - p))^{1/2}$ where n is the number of data and p is the number of parameters refined.

Table S1. (Continued from the previous page)

complex	**4**	**5**	**7**	**8**
formula	$C_{69}H_{110}Cl_4Li_2N_2O_7Zn_2 \times C_6H_{14}$	$C_{57}H_{80}N_2O_3Zn_2 \times 2OEt_2$	$C_{89}H_{96}N_4O_{10}Zn_4 \times C_7H_8$	$0.5C_{48}H_{64}N_2O_2Zn \times OEt_2$
Fw, g/mol	1409.10	1078.11	1080.02	457.31
temperature	100(2)	100(2)	100(2)	100(2)
cryst syst	monoclinic	triclinic	monoclinic	orthorhombic
space group	$P2_1/c$	*P-1*	$P2_1/c$	*P*bcn
color	yellow	yellow	yellow	yellow
Z	4	2	4	8
a, Å	16.4922(6)	14.0422(16)	15.2656(7)	18.7049(11)
b, Å	27.6893(11)	14.7543(18)	24.0925(10)	11.8936(7)
c, Å	18.6758(8)	14.7543(18)	16.2518(7)	23.2743(14)
α, deg	90.00	94.571(6)	90.00	90.00
β, deg	113.206(2)	107.133(5)	91.554(2)	90.00
γ, deg	90.00	106.102(5)	90.00	90.00
V, A^3	7838.4(5)	3072.3(6)	5975.0(5)	5177.8(5)
d_{calcd}, g/cm^3	1.194	1.165	1.201	1.173
μ, mm^{-1}	0.796	0.826	0.850	0.520
2θ, deg	50.26	47.00	52.98	54.92
$R_1{}^a$ (all data)	0.1307	0.1316	0.1088	0.0668
$wR_2{}^b$ (all data)	0.1776	0.1705	0.1059	0.0957
$R_1{}^a$ [(I>2σ)]	0.0607	0.0610	0.0467	0.0375
$wR_2{}^b$ [(I>2σ)]	0.1556	0.1532	0.0945	0.0887
GOF (F^2)	0.933	0.961	0.928	0.945

2. Structures of L^{syn}, L^{anti}, and complex 8

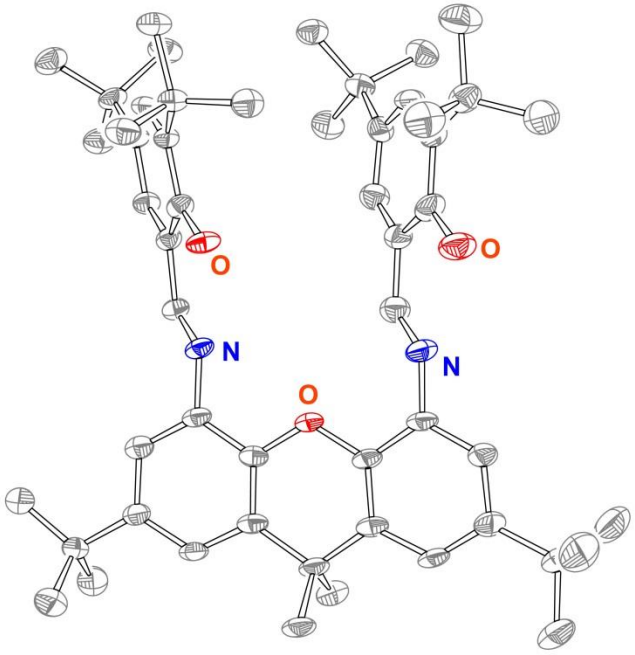

Figure S1. X-ray structure of L^{syn}, 50% probability ellipsoids.

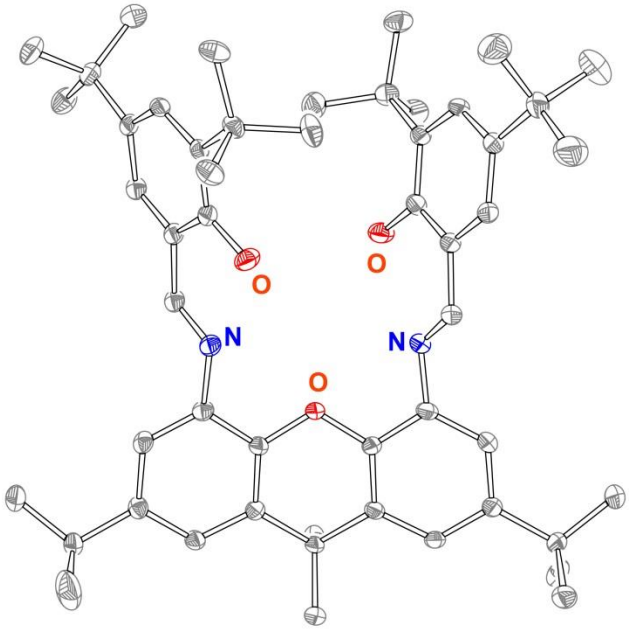

Figure S2. X-ray structure of L^{anti}, 50% probability ellipsoids.

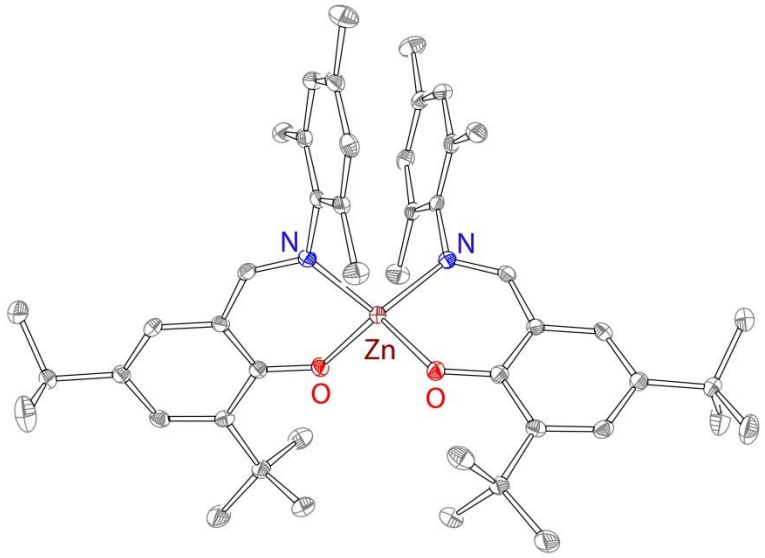

Figure S3. X-ray structure of **8**, 50% probability ellipsoids.

3. NMR spectra

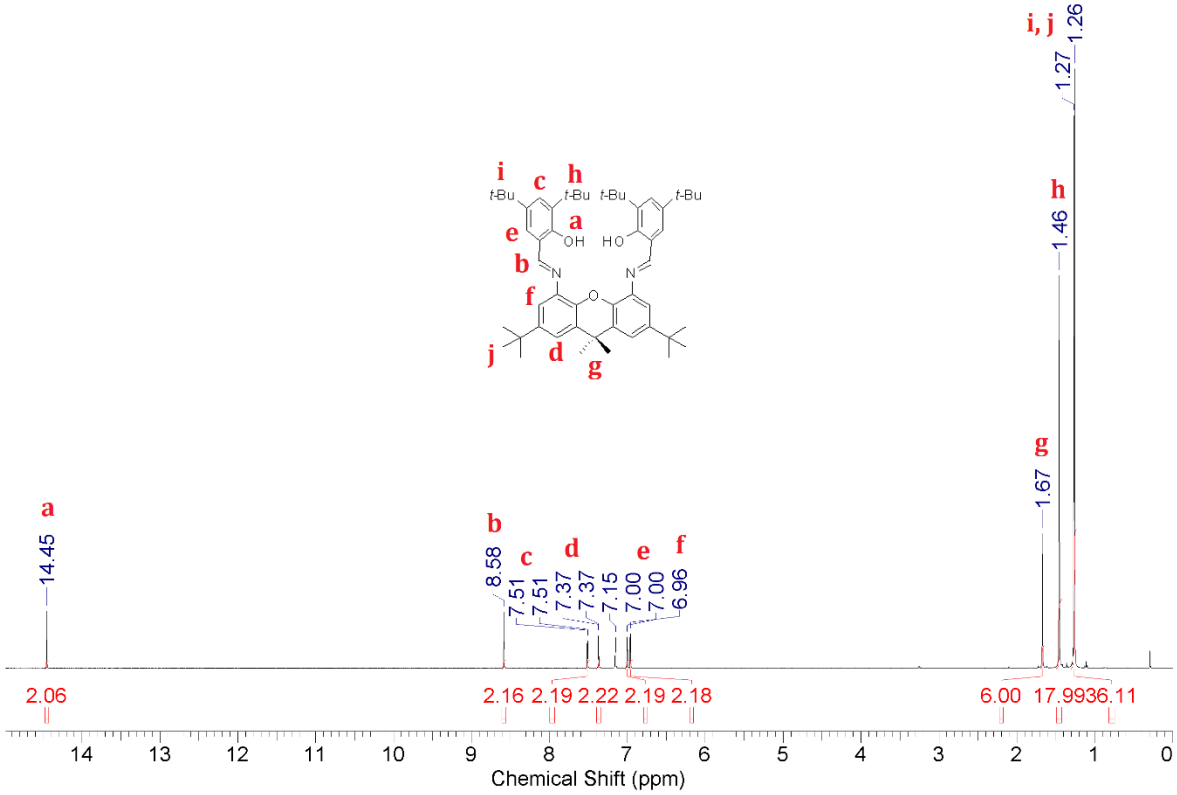

Figure S4. ^{1}H NMR of L (C_6D_6, 400 MHz).

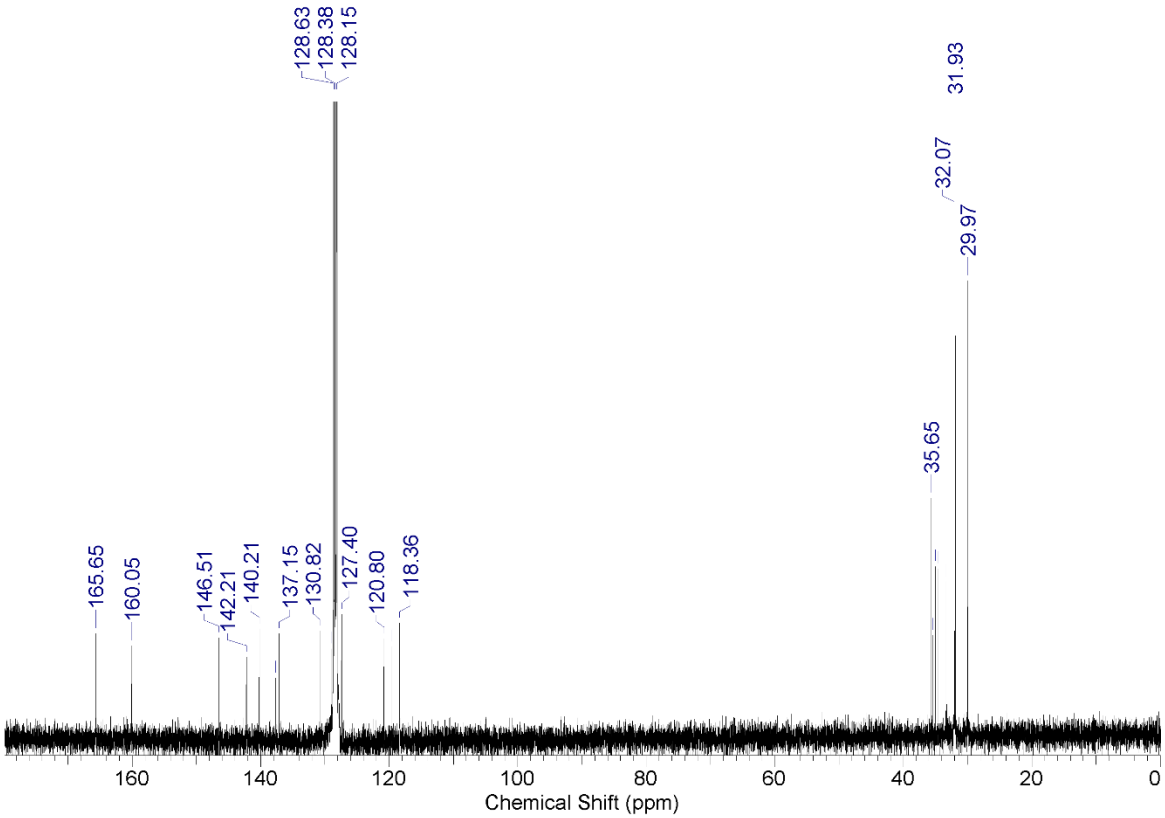

Figure S5. ^{13}C NMR of L (C_6D_6, 100 MHz).

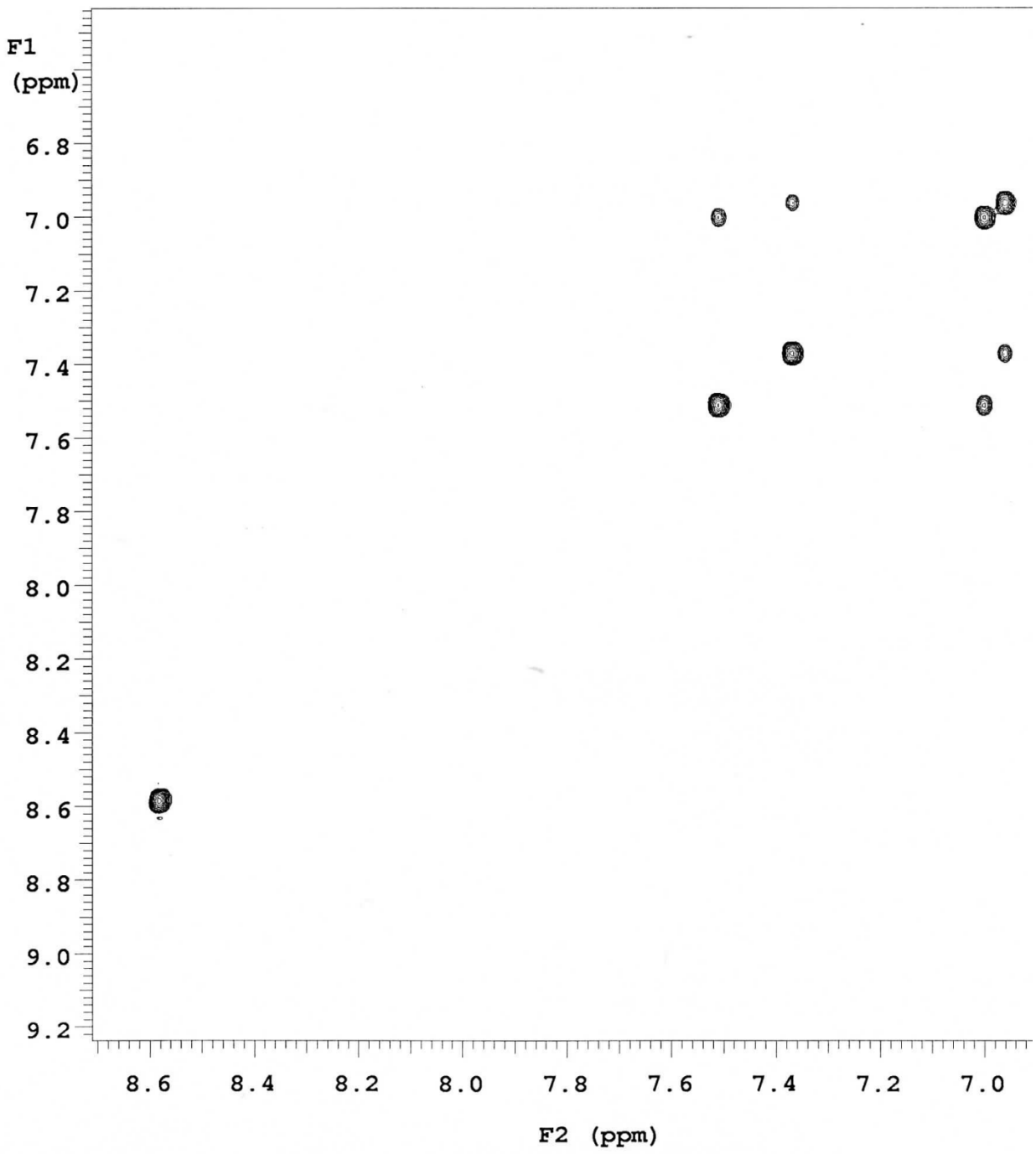

Figure S6. TOCSY NMR of L (C_6D_6, 400 MHz) – Aromatic Region.

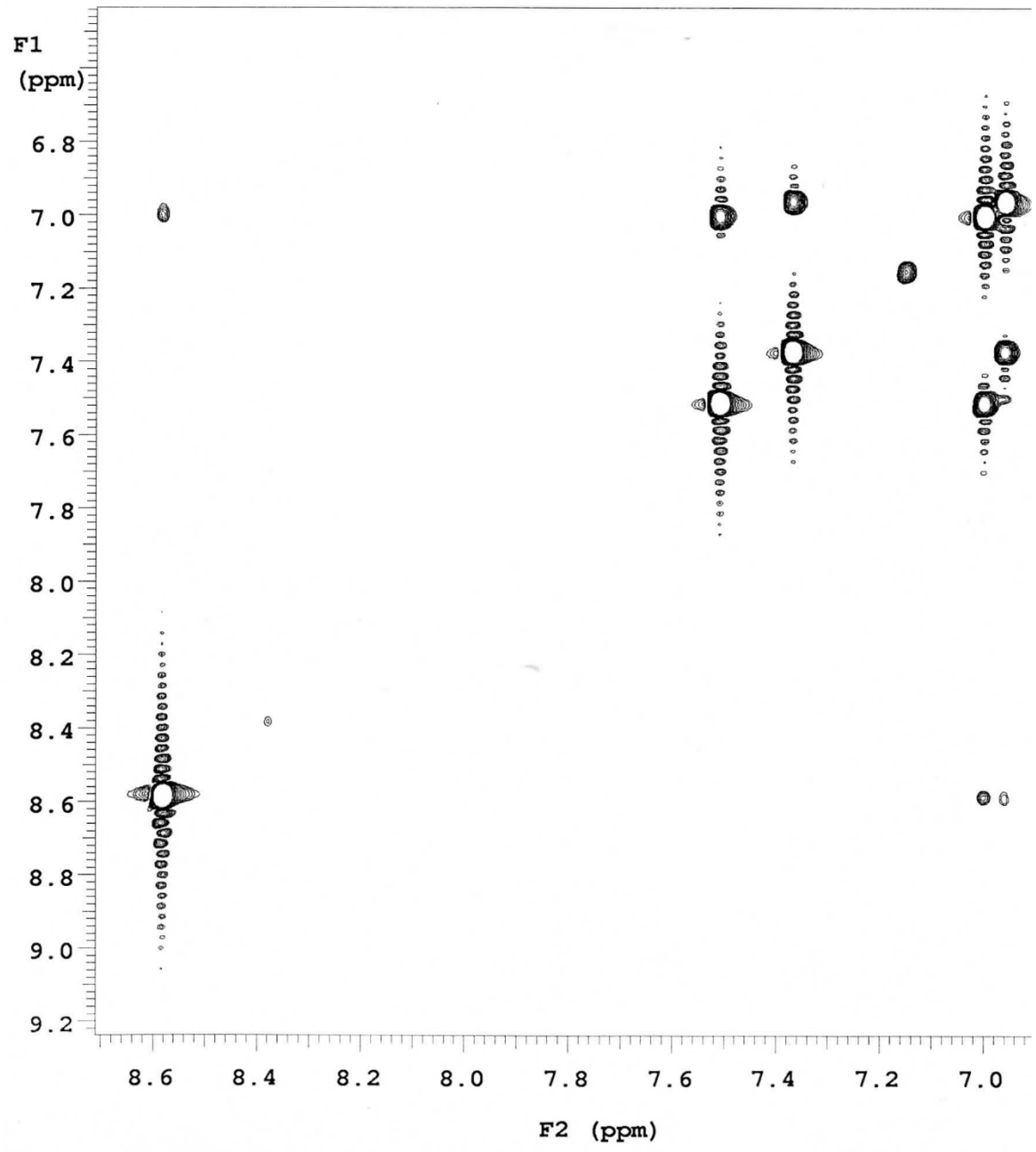

Figure S7. TOCSY NMR of L (C_6D_6, 400 MHz) – Aromatic Region (Zoomed).

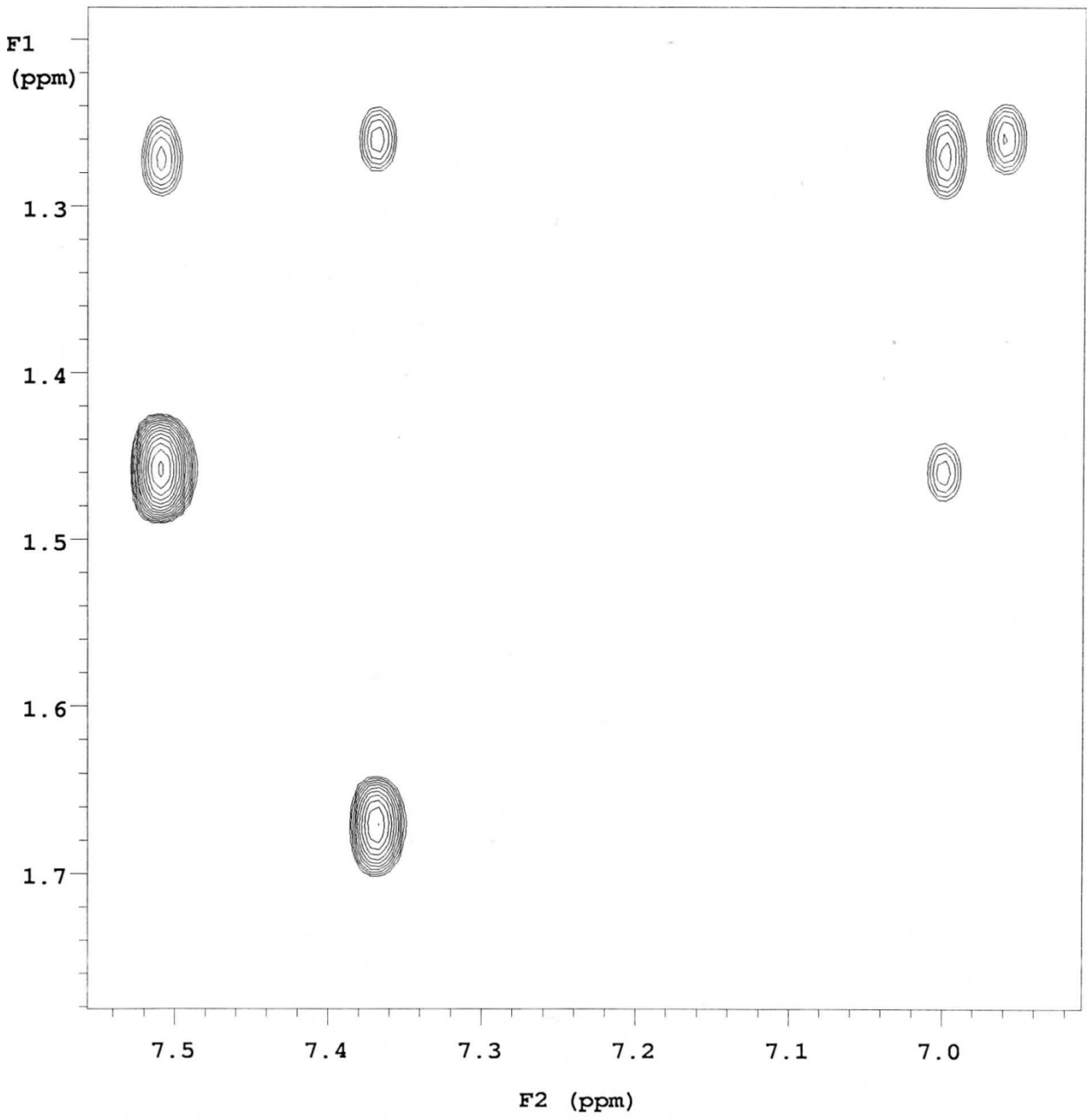

Figure S8. TOCSY NMR of L (C_6D_6, 400 MHz) – Aromatic/Aliphatic.

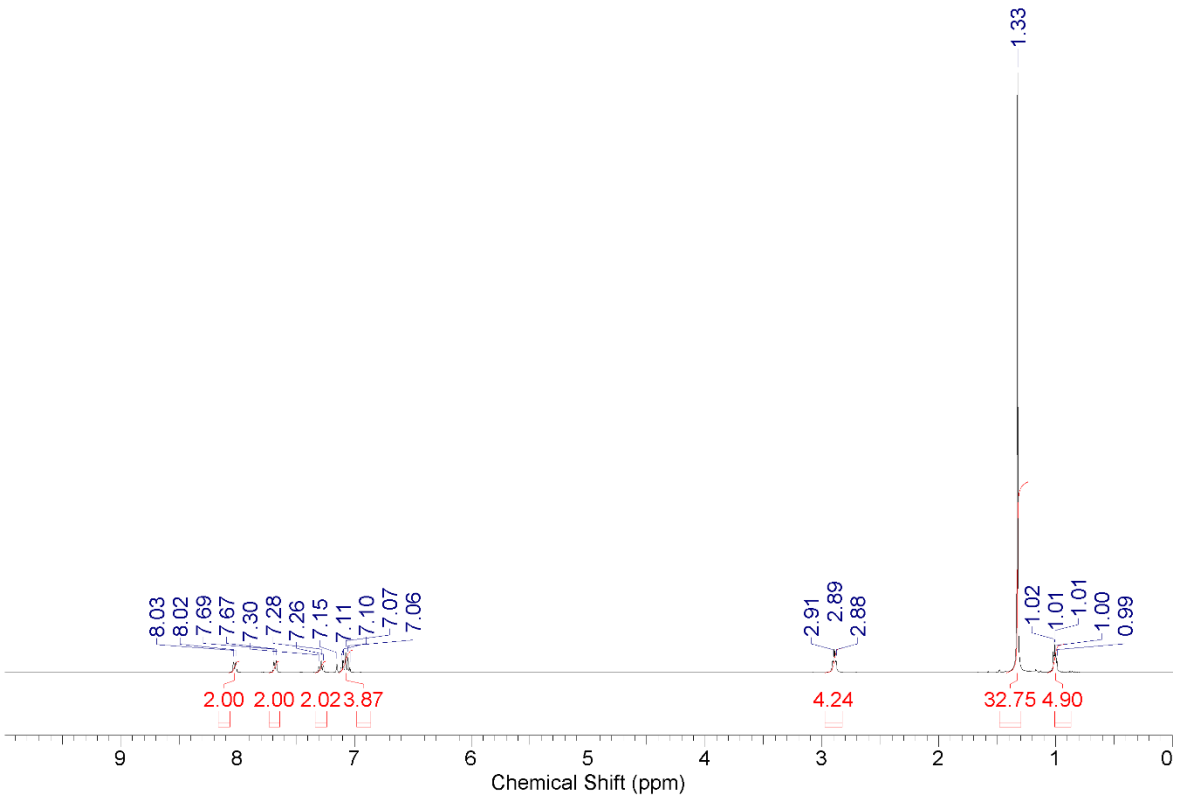

Figure S9. ^{1}H NMR of **1** (C_6D_6, 400 MHz).

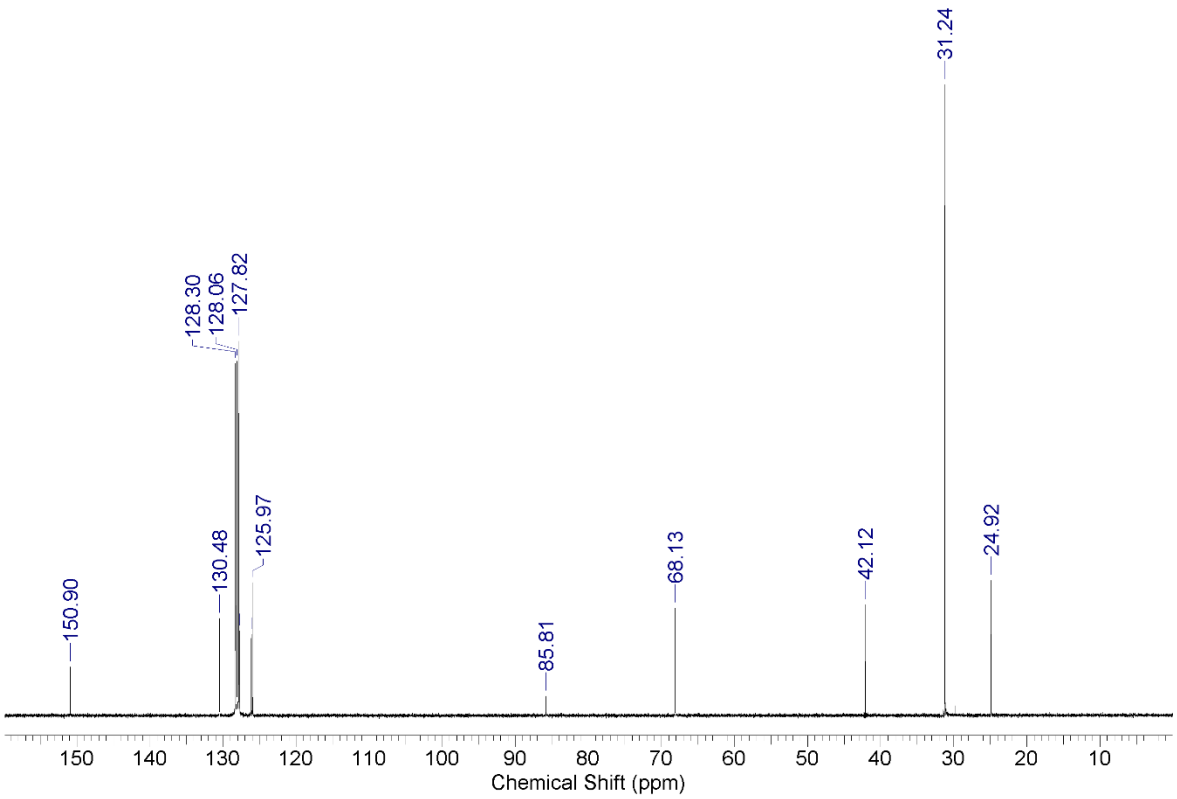

Figure S10. ^{13}C NMR of **1** (C_6D_6, 100 MHz).

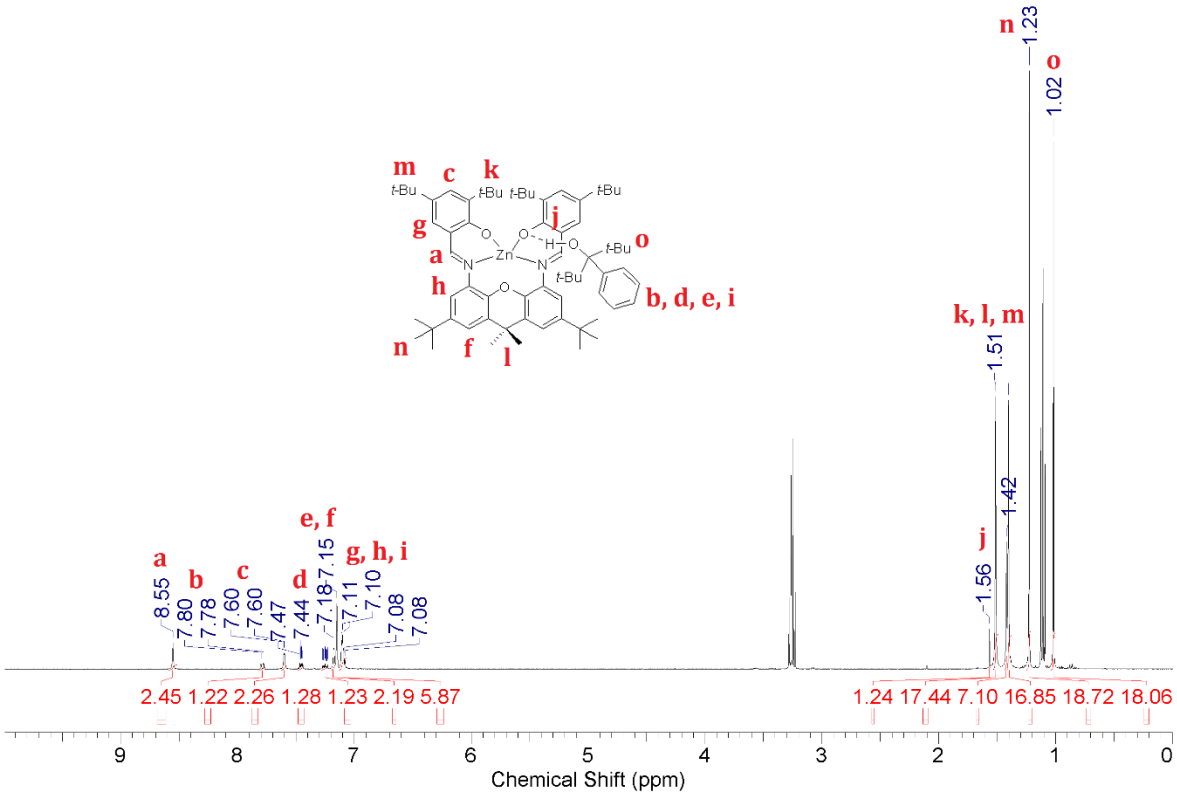

Figure S11. ^{1}H NMR of **2**•HOR (C_6D_6, 400 MHz).

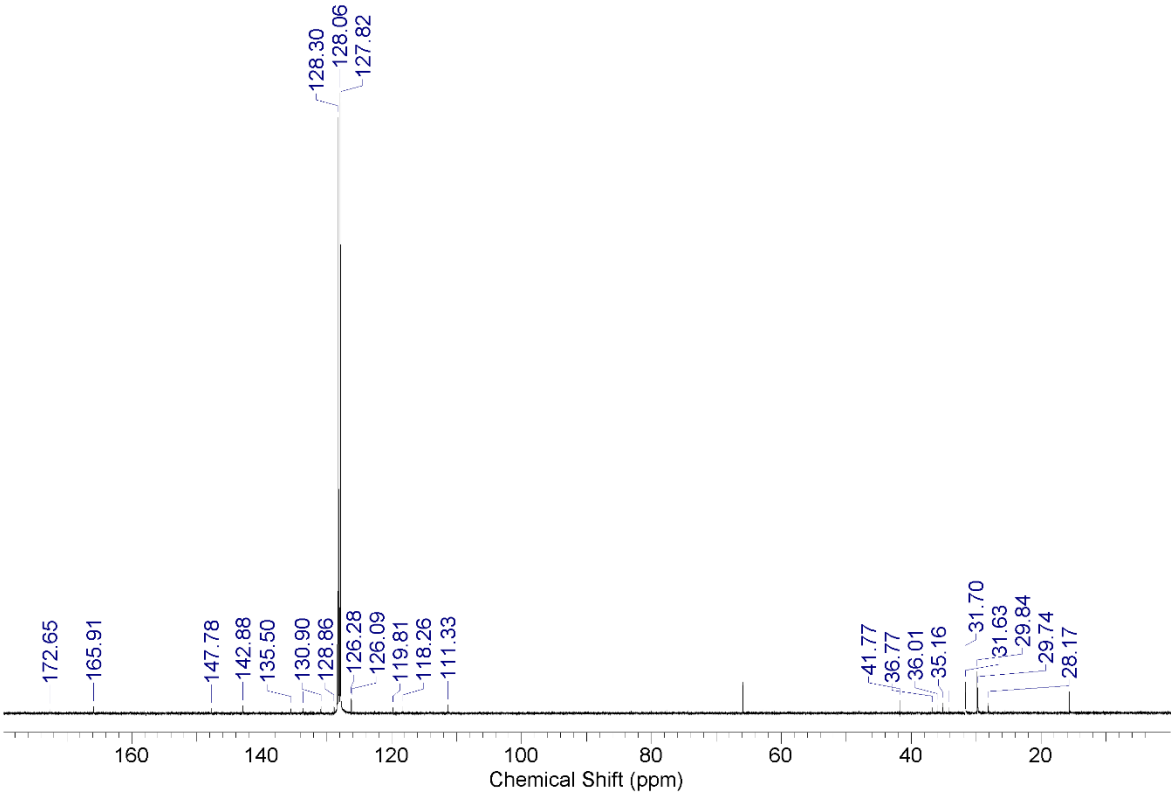

Figure S12. ^{13}C NMR of **2**•HOR (C_6D_6, 100 MHz).

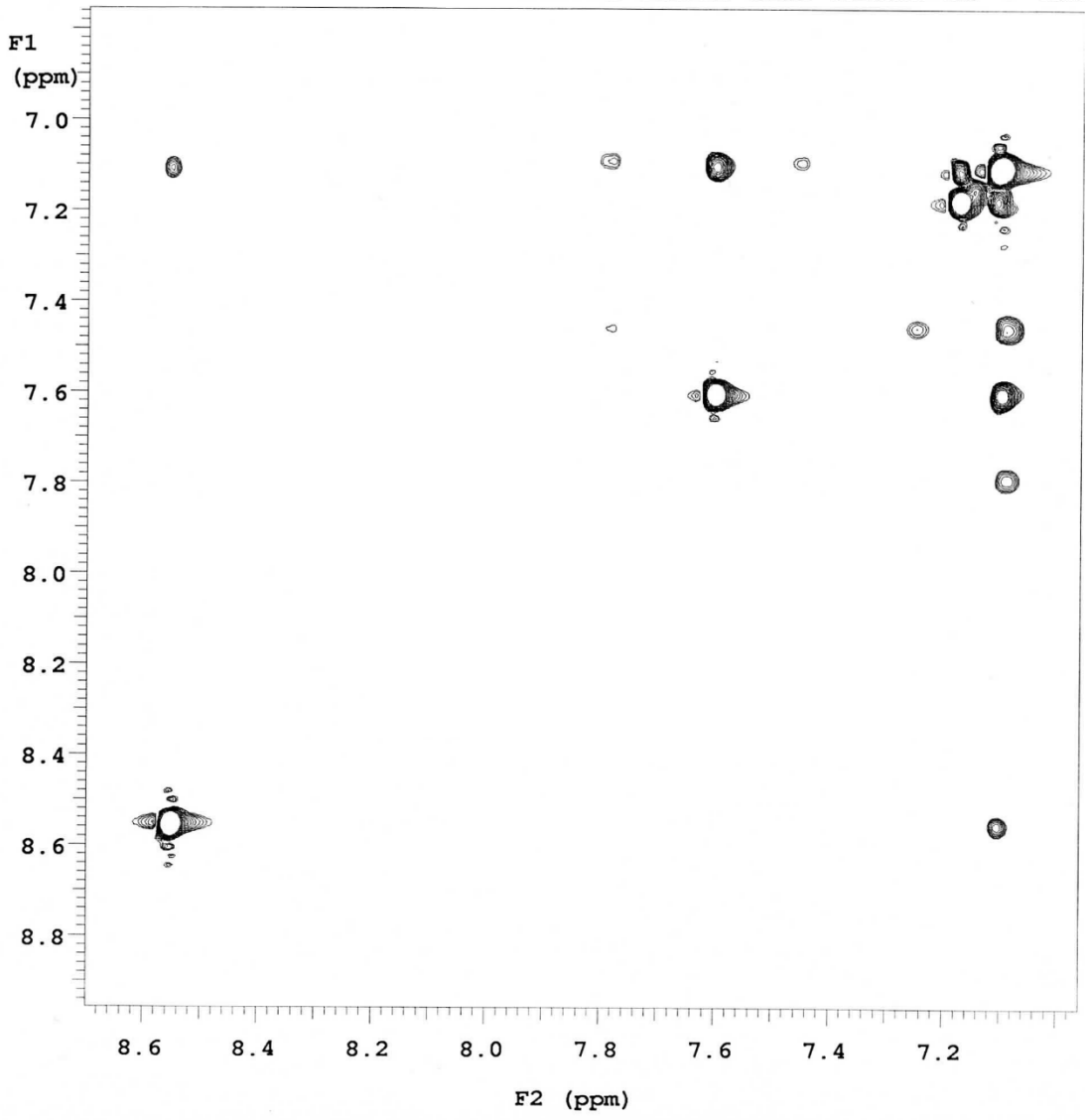

Figure S13. TOCSY NMR of **2**•HOR (C_6D_6, 400 MHz) – Aromatic Region.

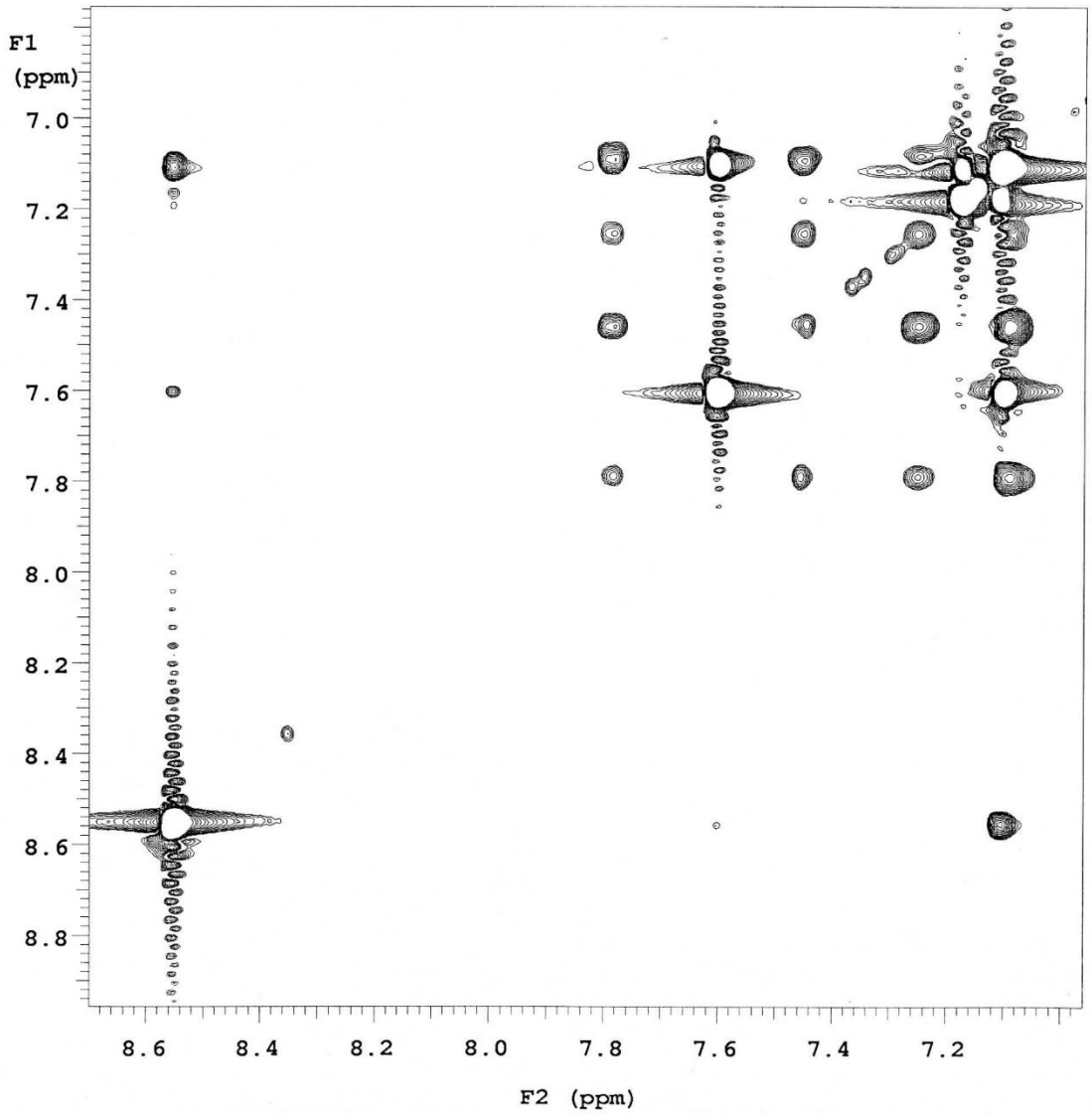

Figure S14. TOCSY NMR of **2**•HOR (C_6D_6, 400 MHz) – Aromatic Region (Zoomed).

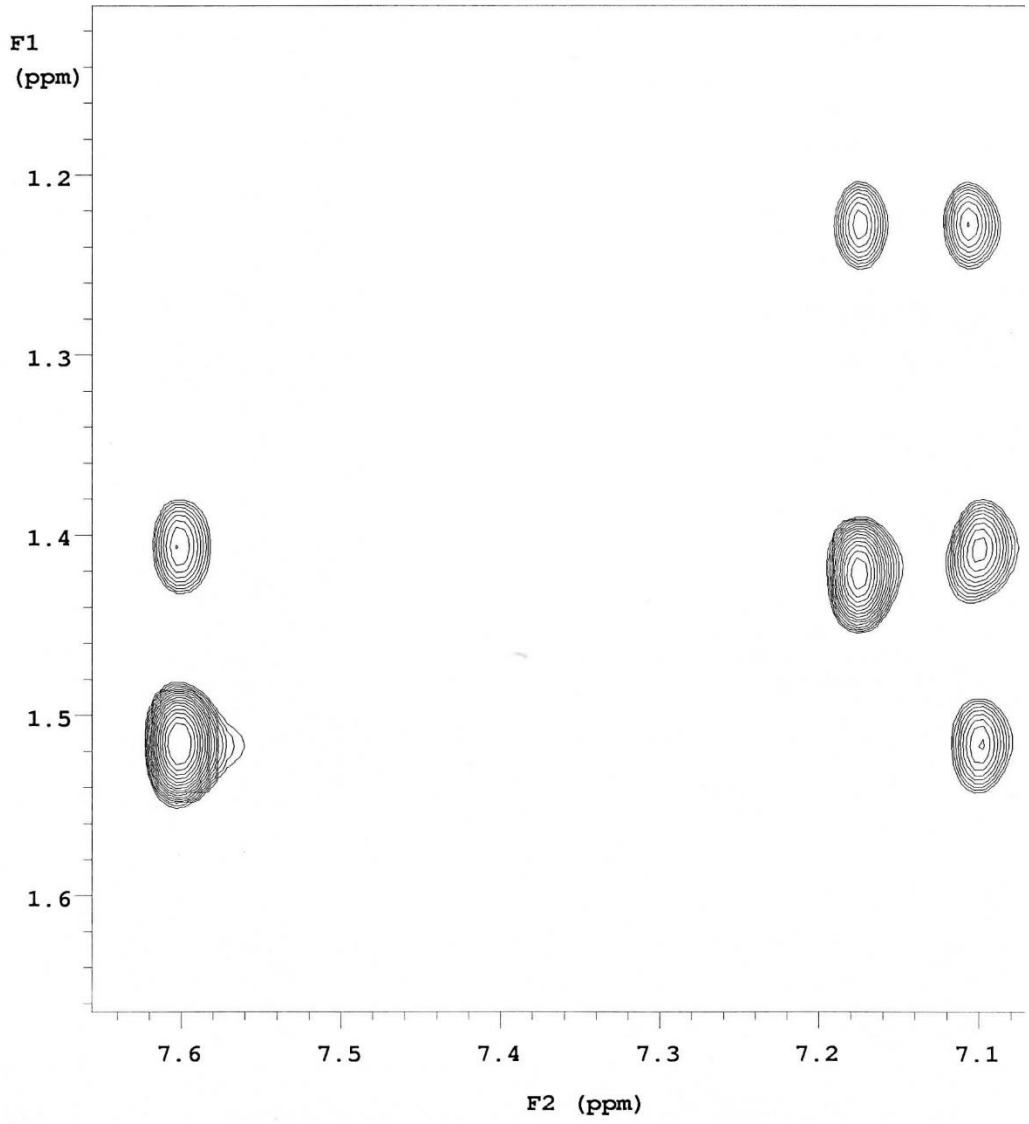

Figure S15. TOCSY NMR of **2**•HOR (C_6D_6, 400 MHz) – Aromatic/Aliphatic.

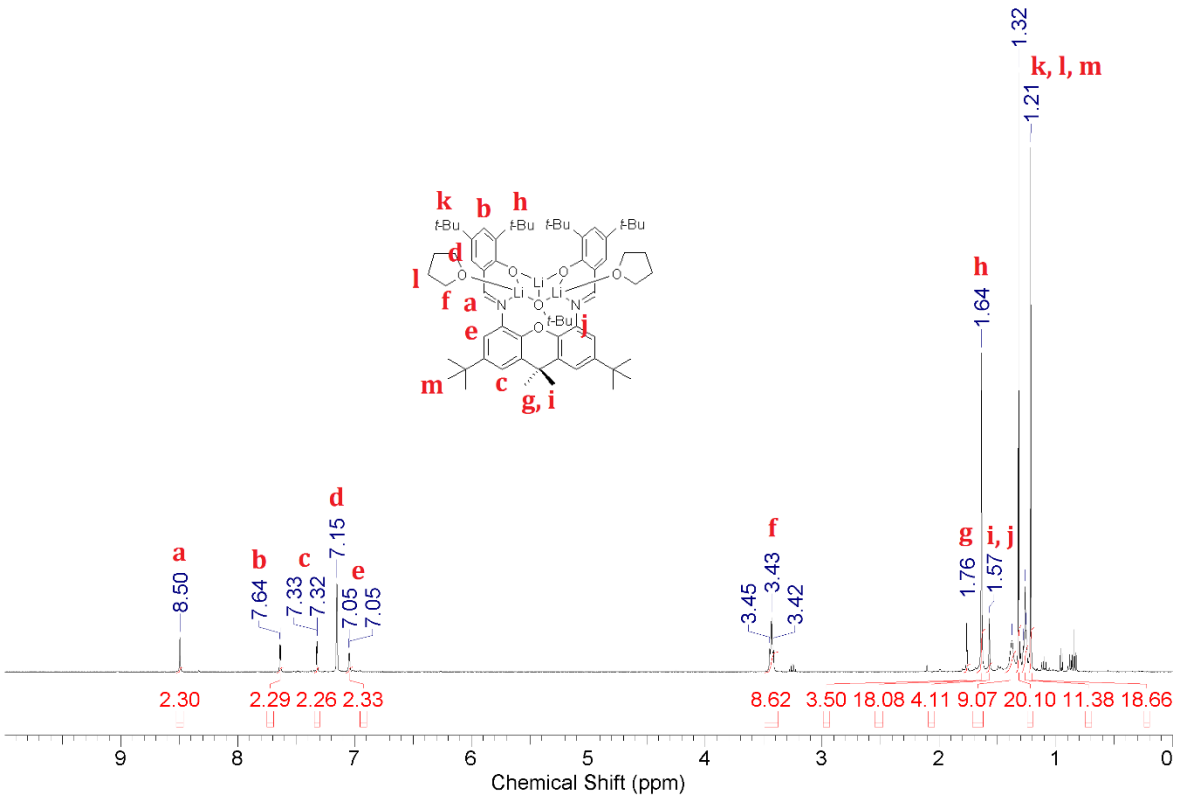

Figure S16. ^{1}H NMR of **3** (C_6D_6, 400 MHz).

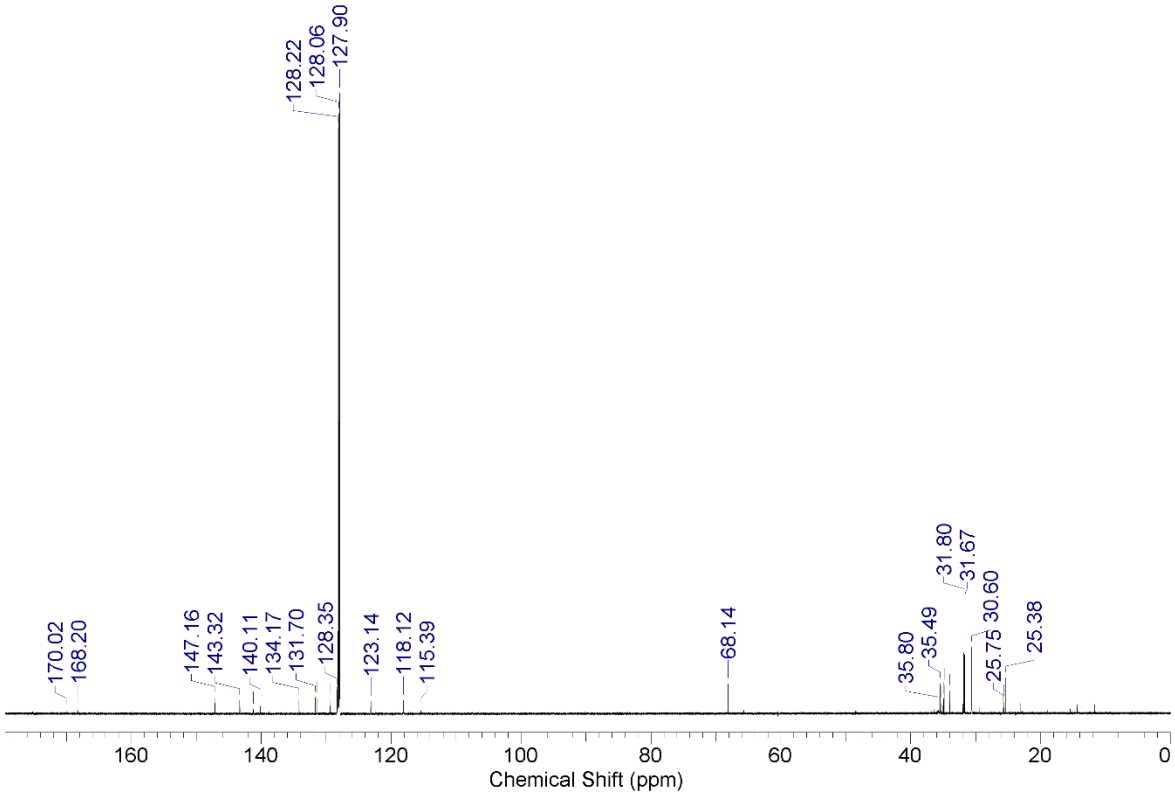

Figure S17. ^{13}C NMR of **3** (C_6D_6, 100 MHz).

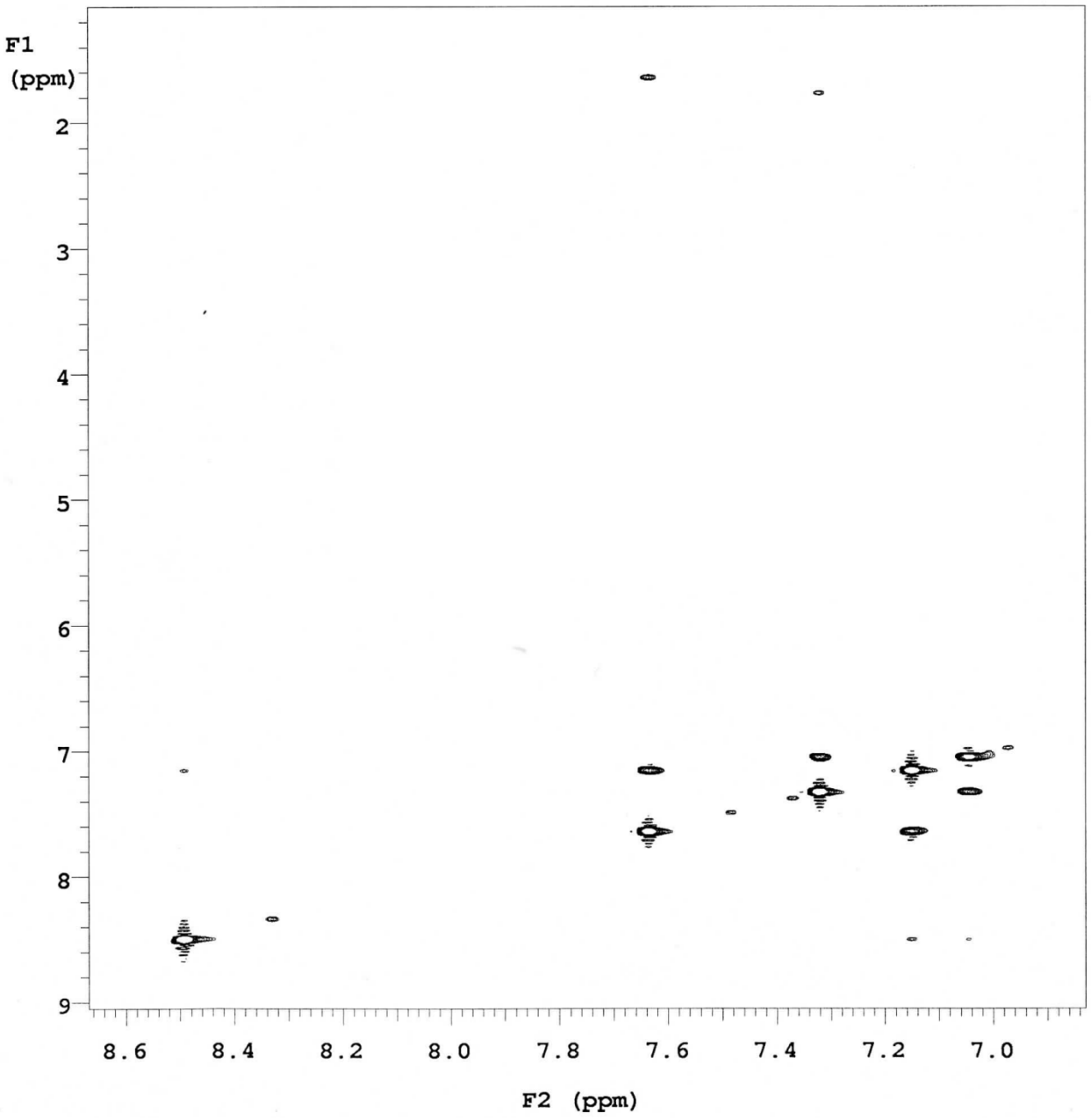

Figure S18. TOCSY NMR of **3** (C_6D_6, 400 MHz) – Aromatic/Aliphatic.

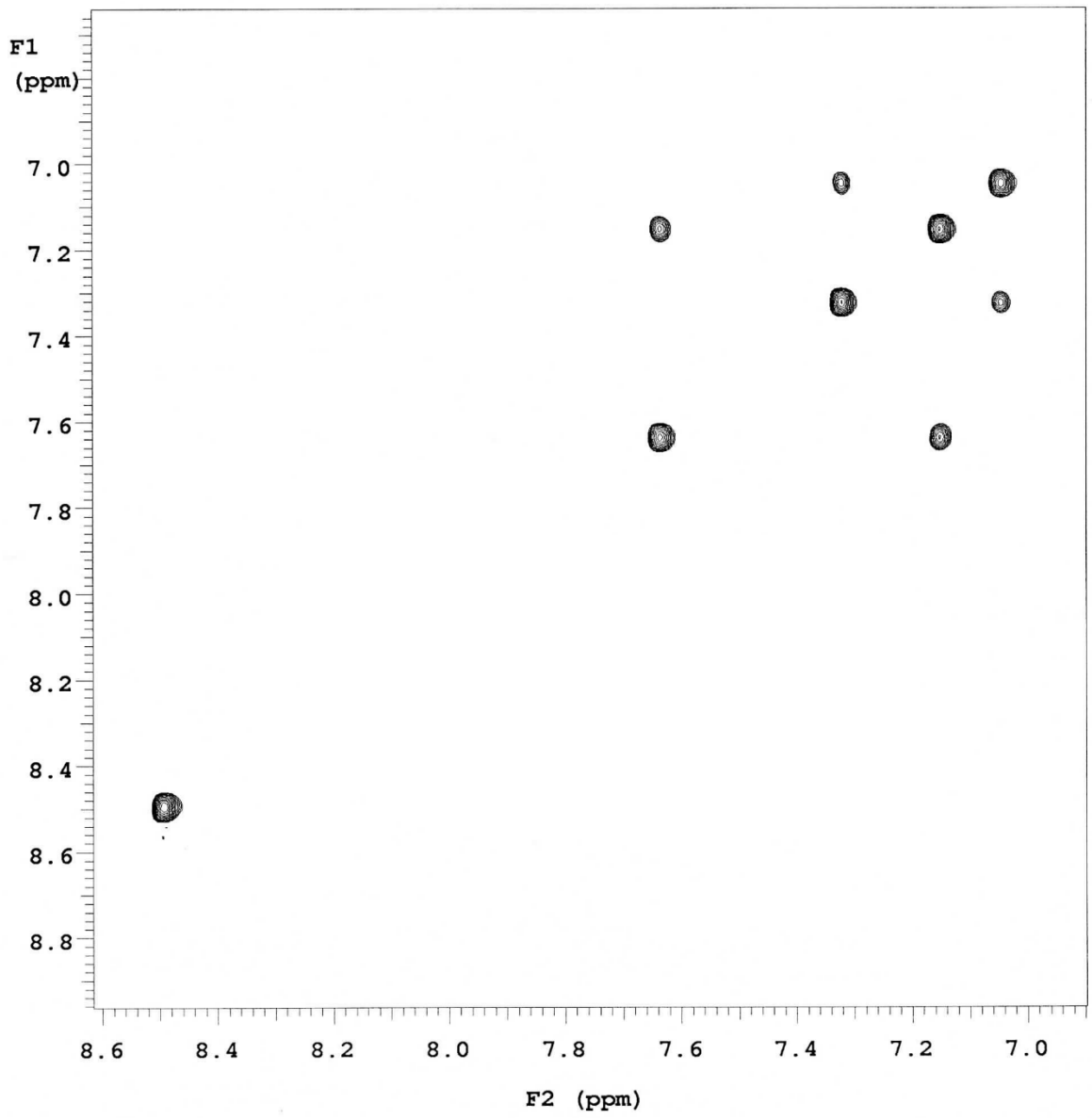

Figure S19. TOCSY NMR of **3** (C_6D_6, 400 MHz) – Aromatic Region.

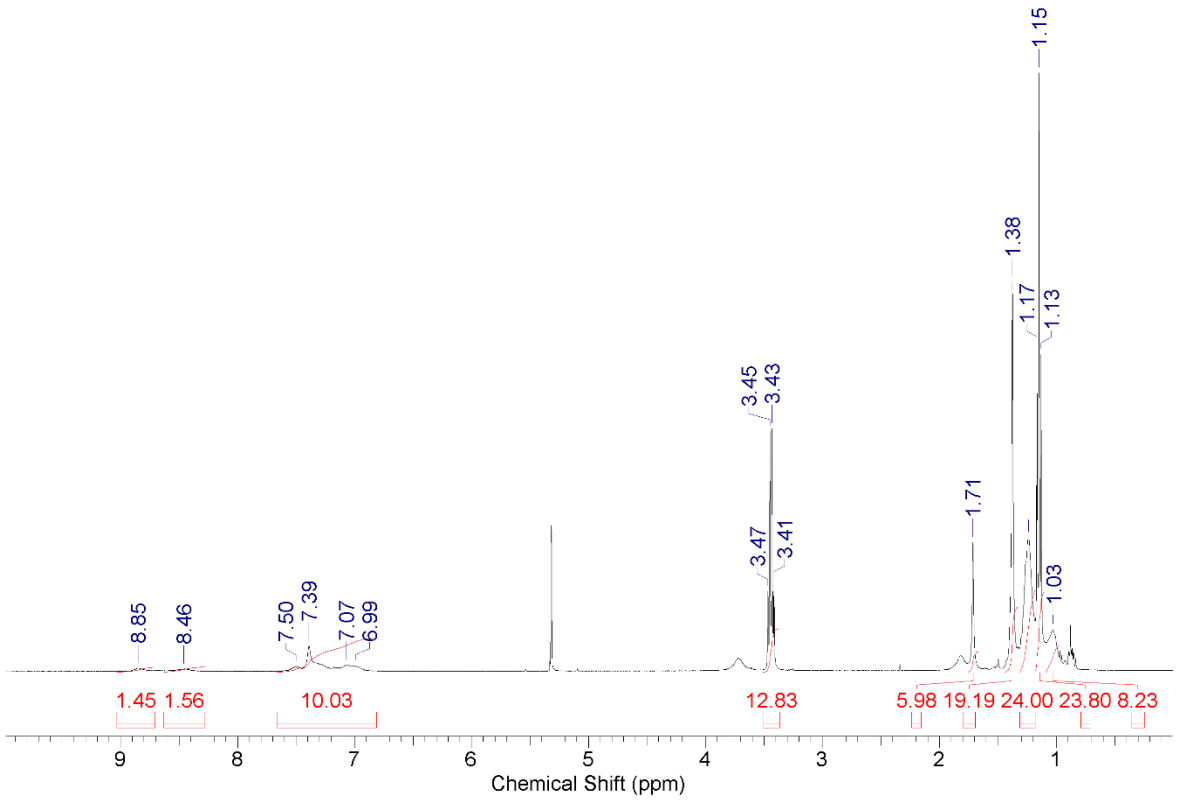

Figure S20. ^{1}H NMR of **4** (C_6D_6, 400 MHz).

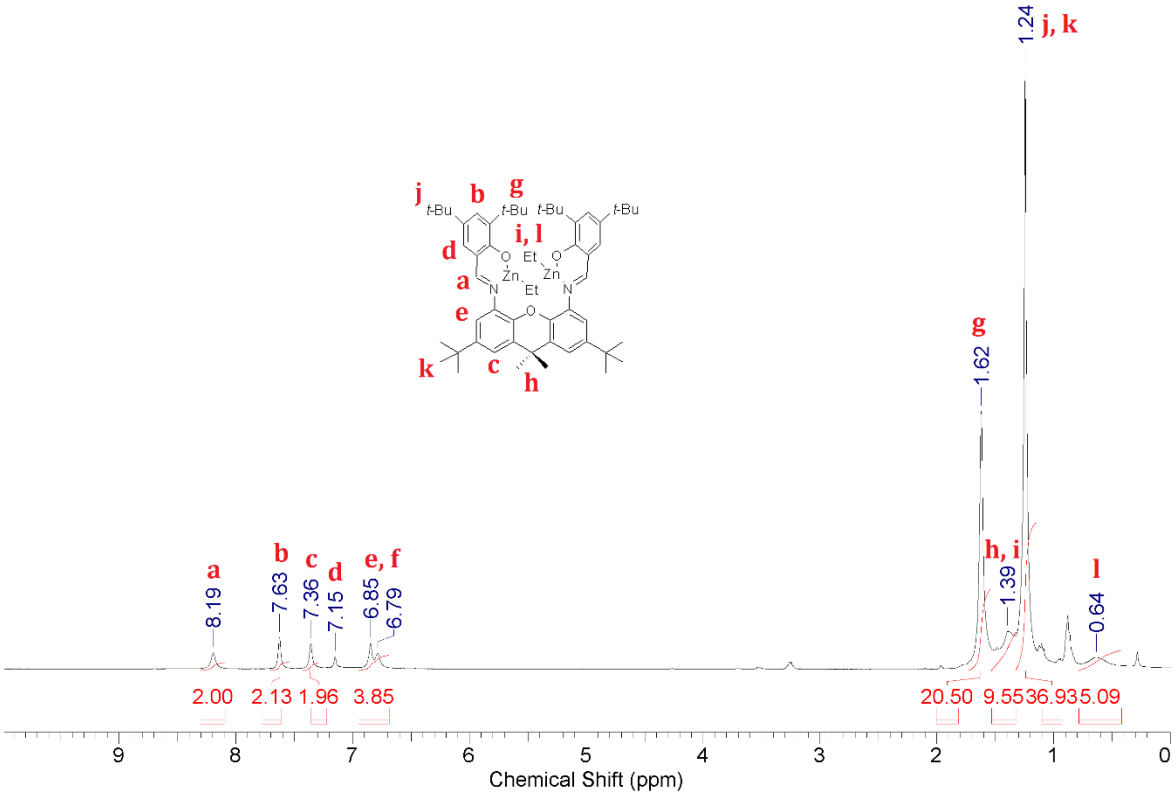

Figure S21. ^{1}H NMR of **5** (C_6D_6, 400 MHz).

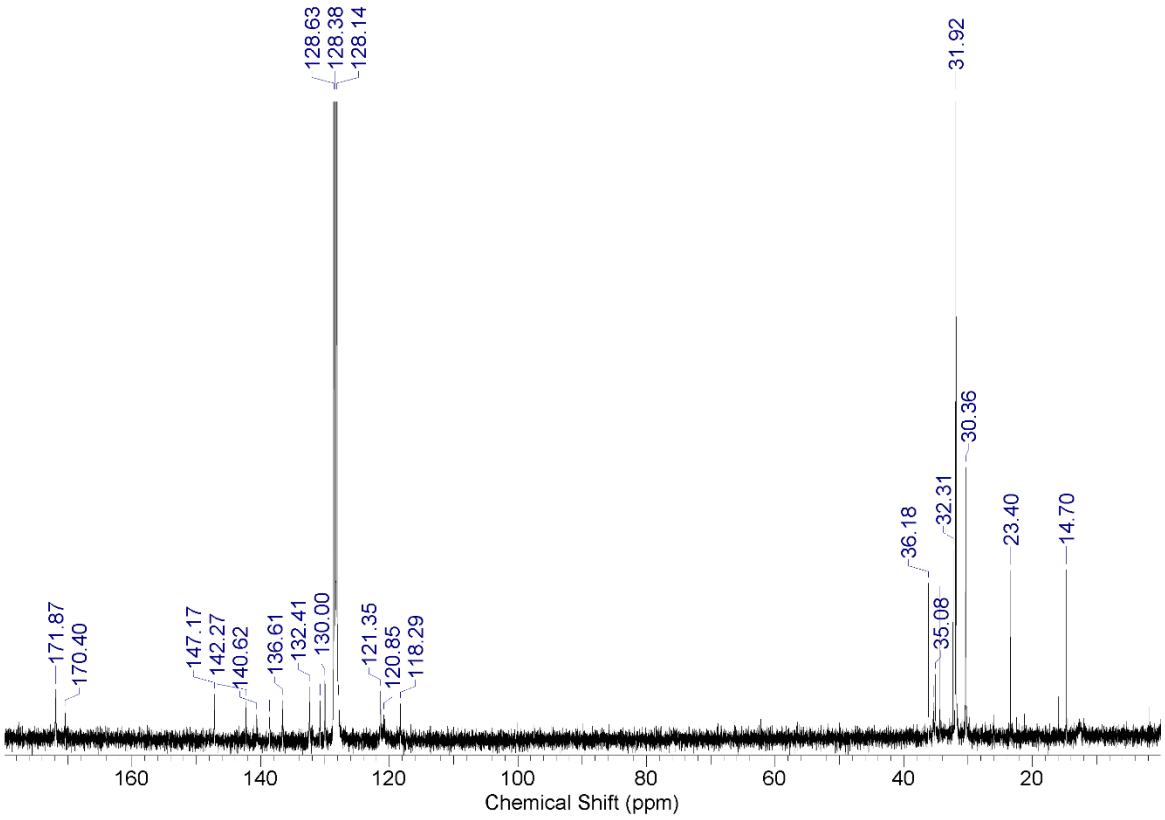

Figure S22. ^{13}C NMR of **5** (C_6D_6, 100 MHz).

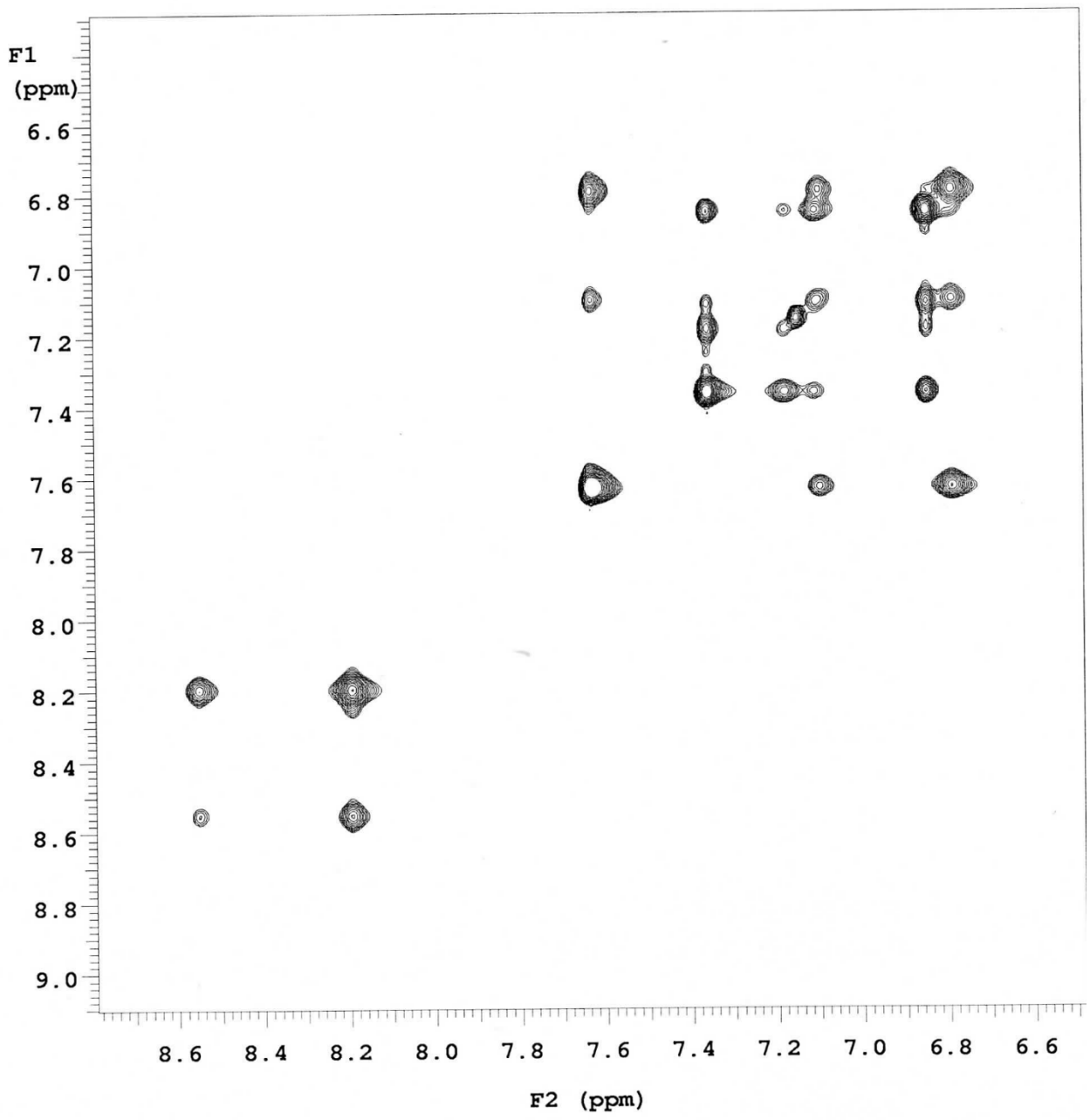

Figure S23. TOCSY NMR of **5** (C_6D_6, 400 MHz) – Aromatic Region.

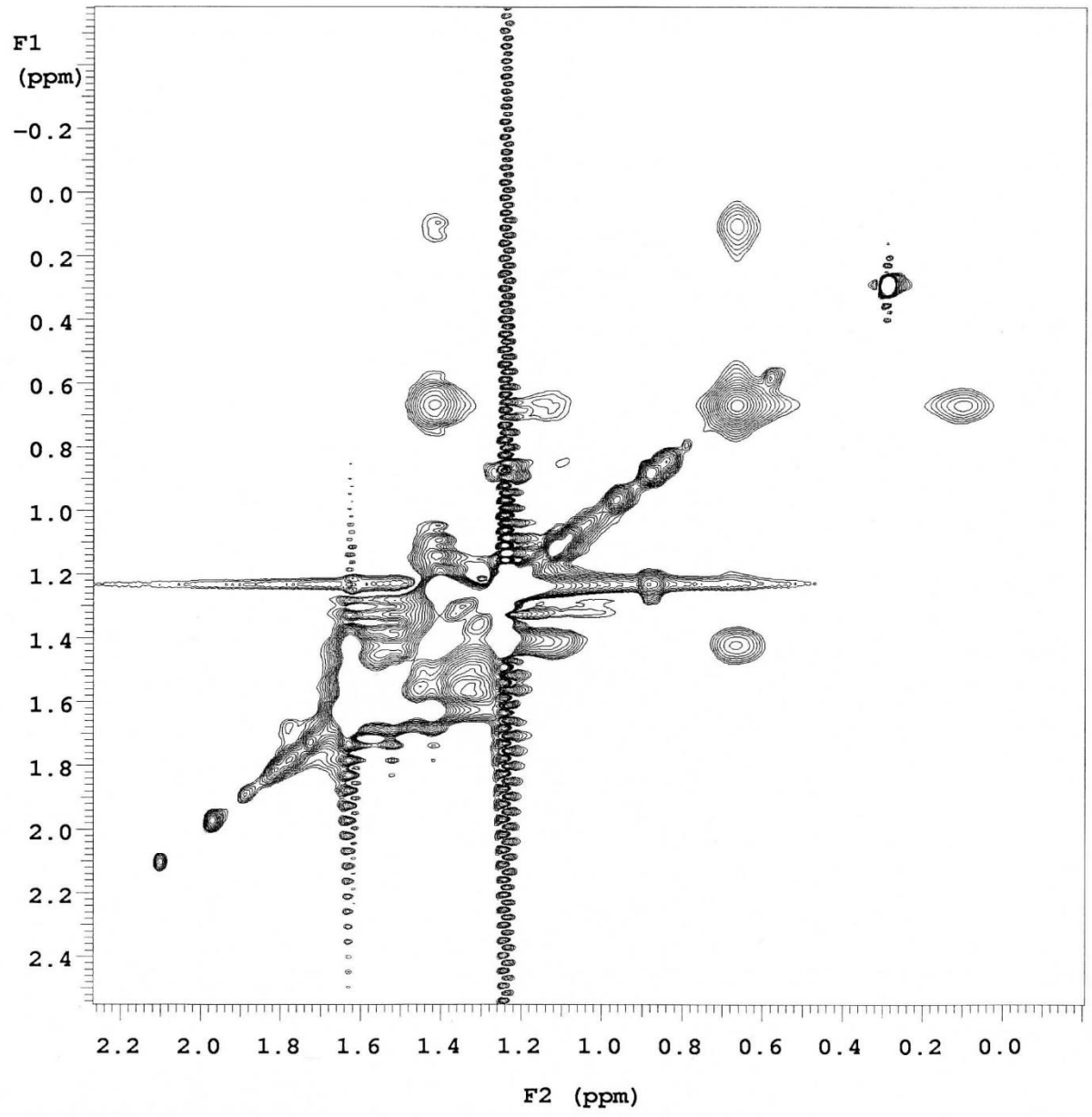

Figure S24. TOCSY NMR of **5** (C_6D_6, 400 MHz) – Aliphatic Region.

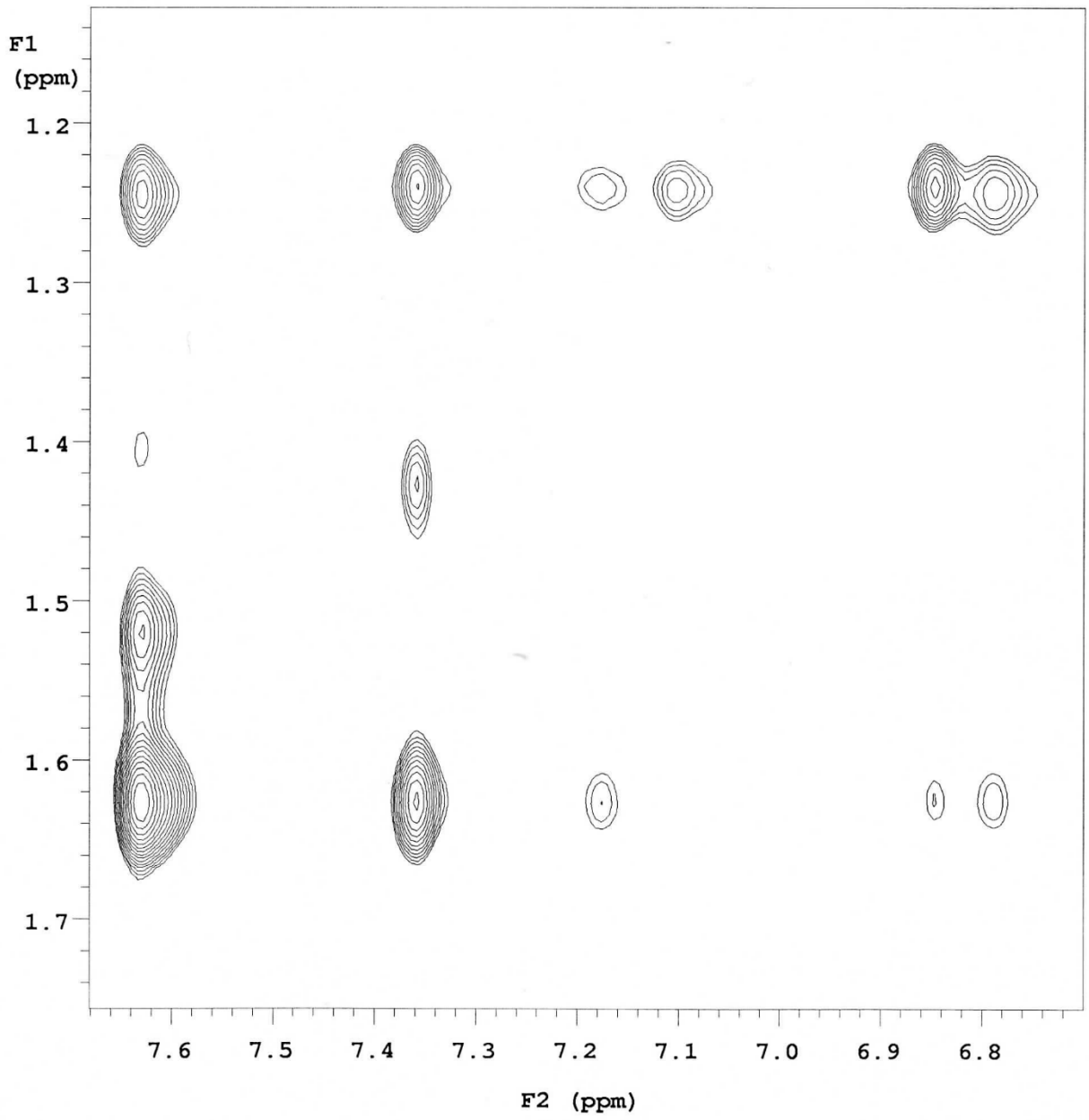

Figure S25. TOCSY NMR of **5** (C_6D_6, 400 MHz) – Aromatic/Aliphatic.

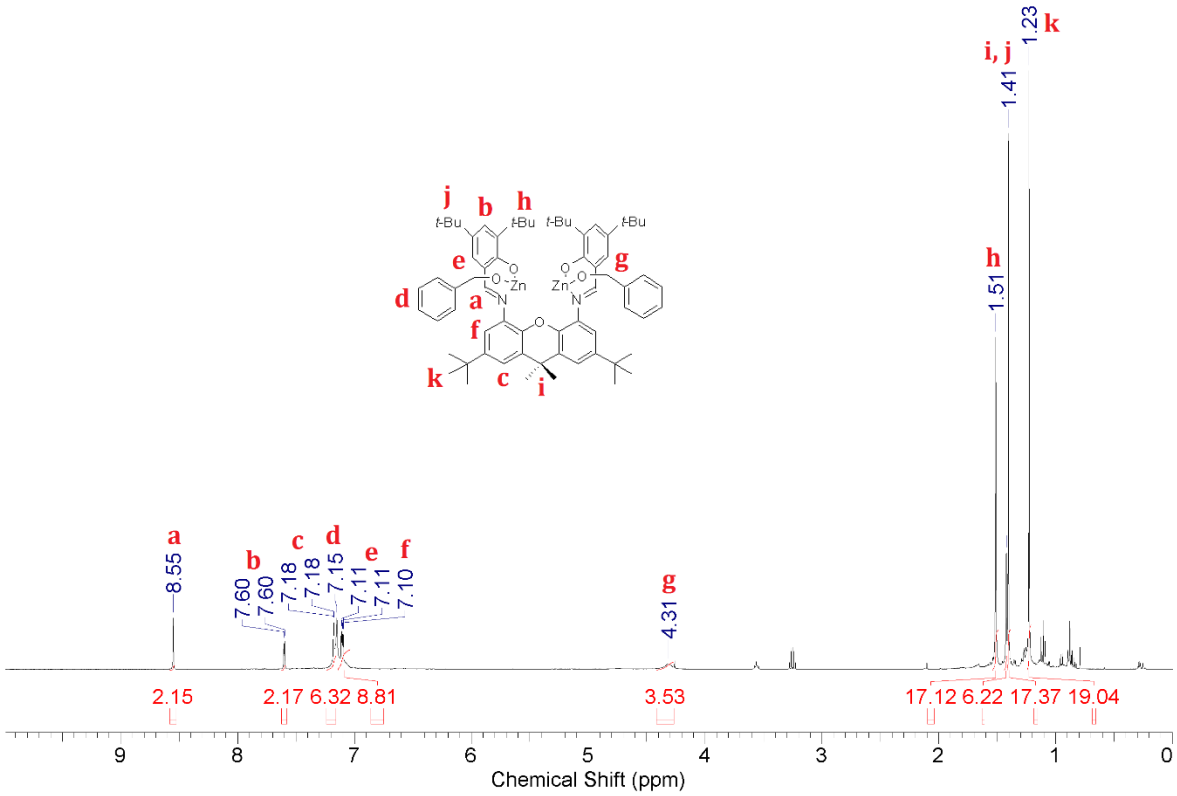

Figure S26. ^{1}H NMR of **6** (C_6D_6, 400 MHz).

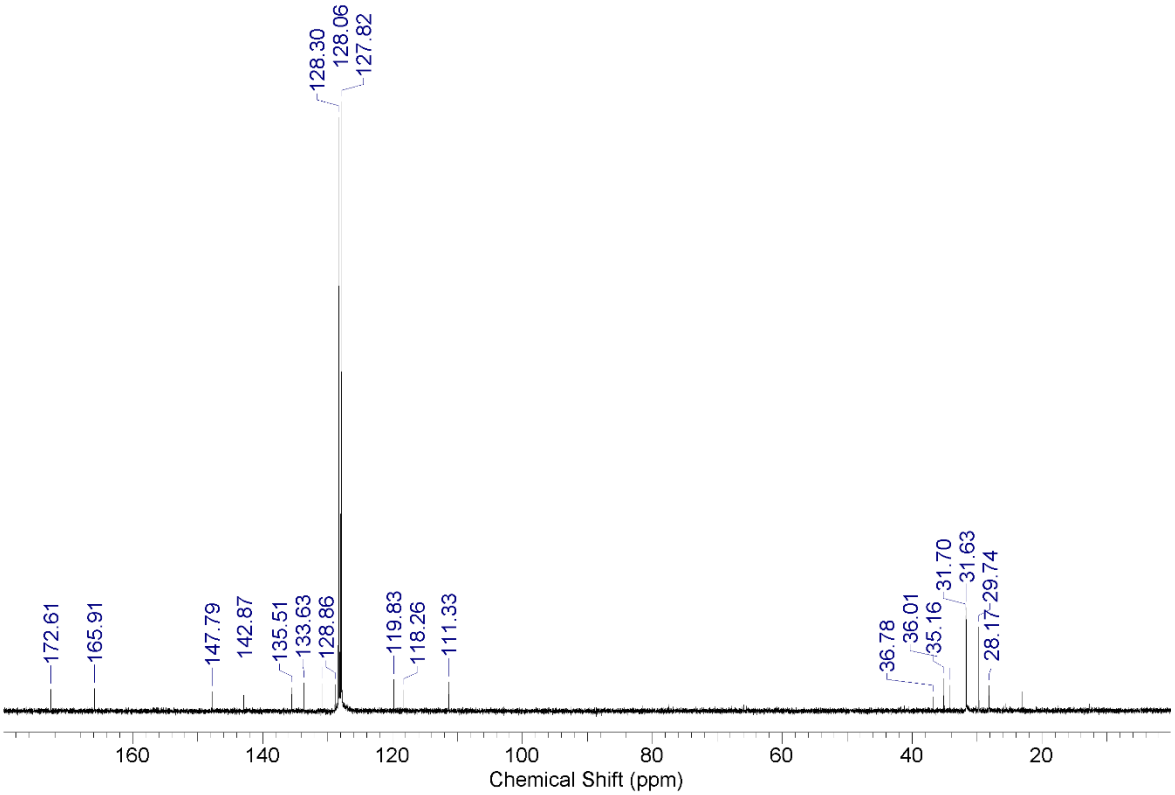

Figure S27. ^{13}C NMR of **6** (C_6D_6, 100 MHz).

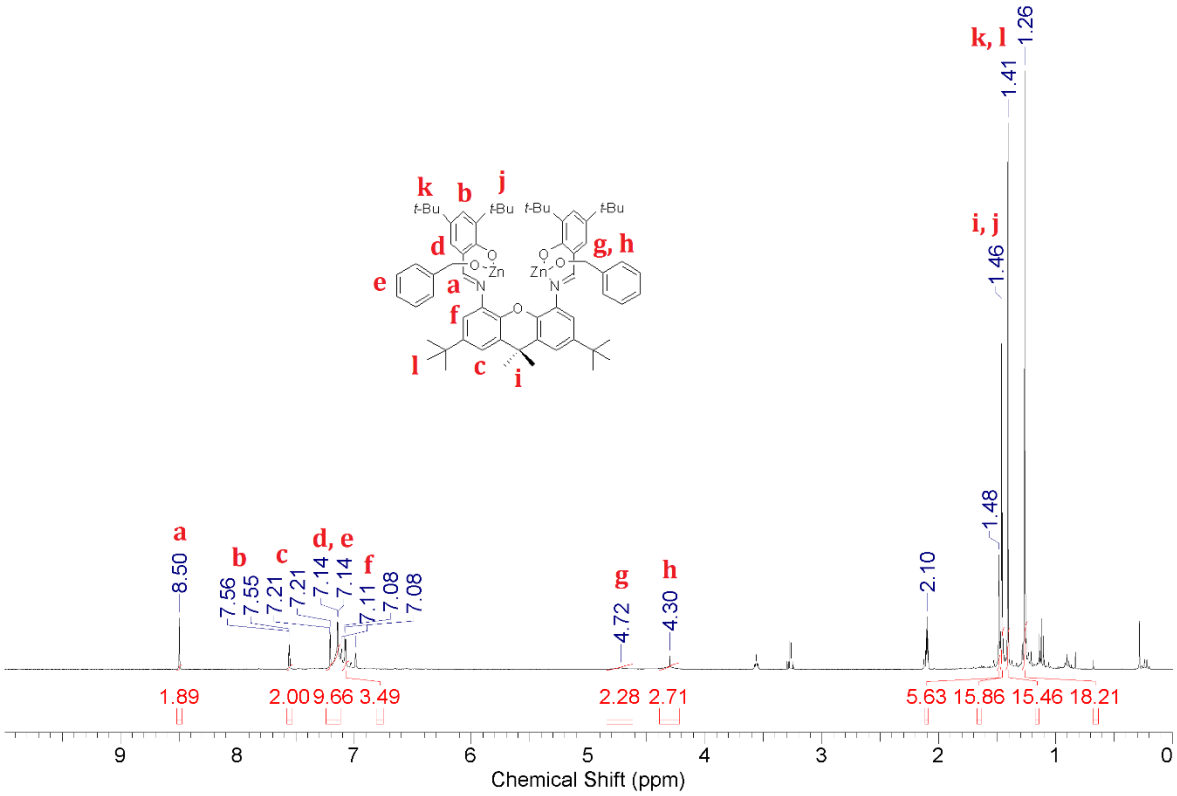

Figure S28. ^{1}H NMR of **6** (C_7D_8, 400 MHz)

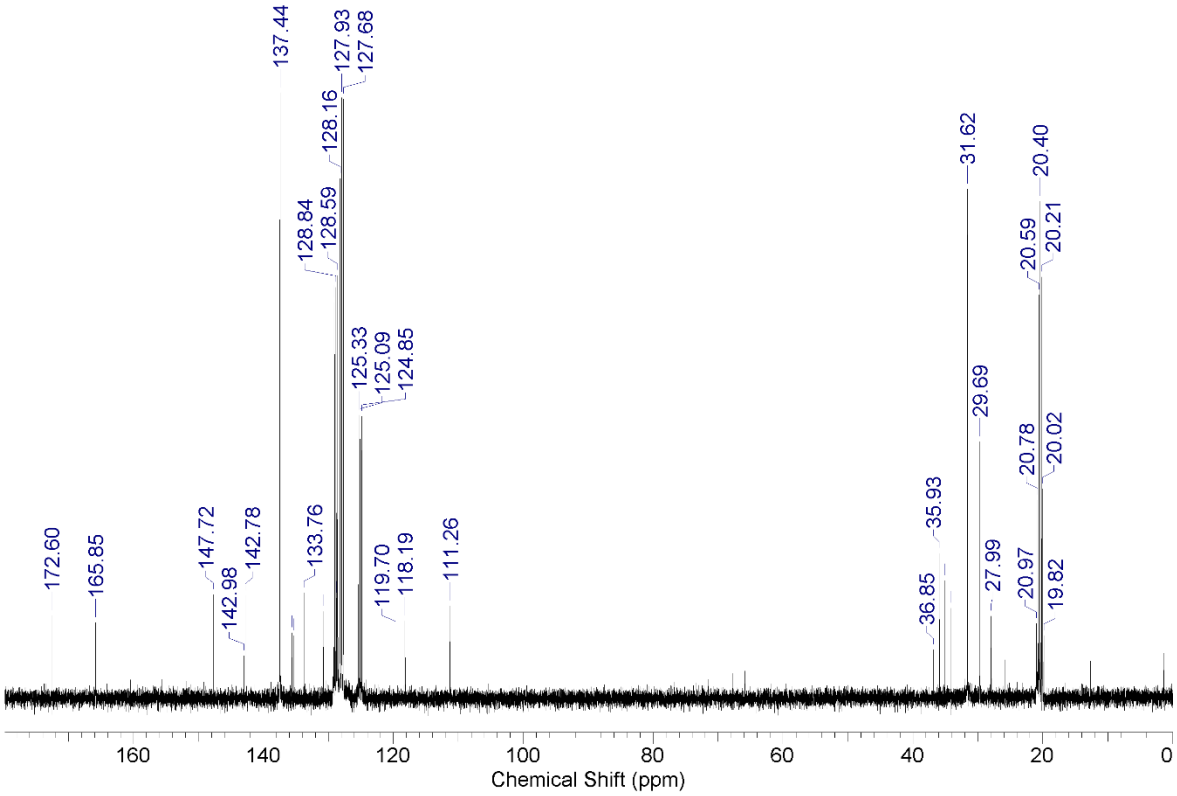

Figure S29. ^{13}C NMR of **6** (C_7D_8, 100 MHz).

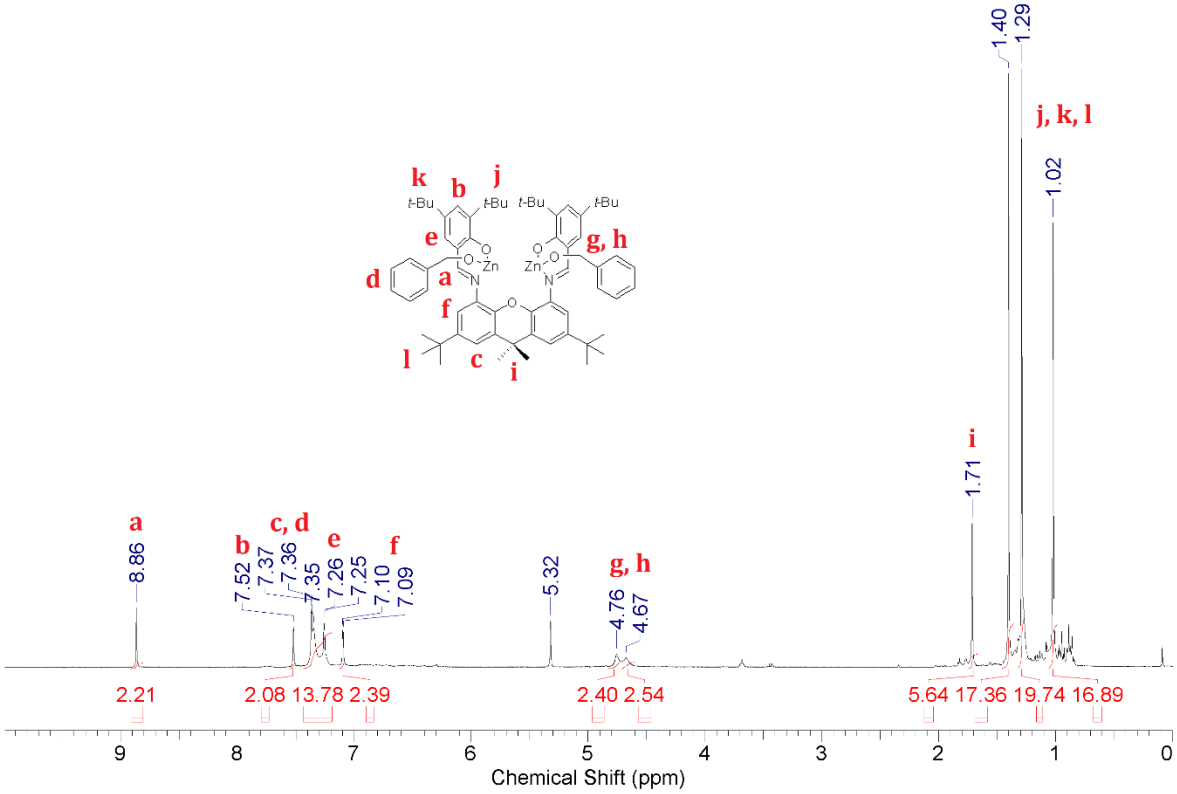

Figure S30. ^{1}H NMR of **6** (CD_2Cl_2, 400 MHz).

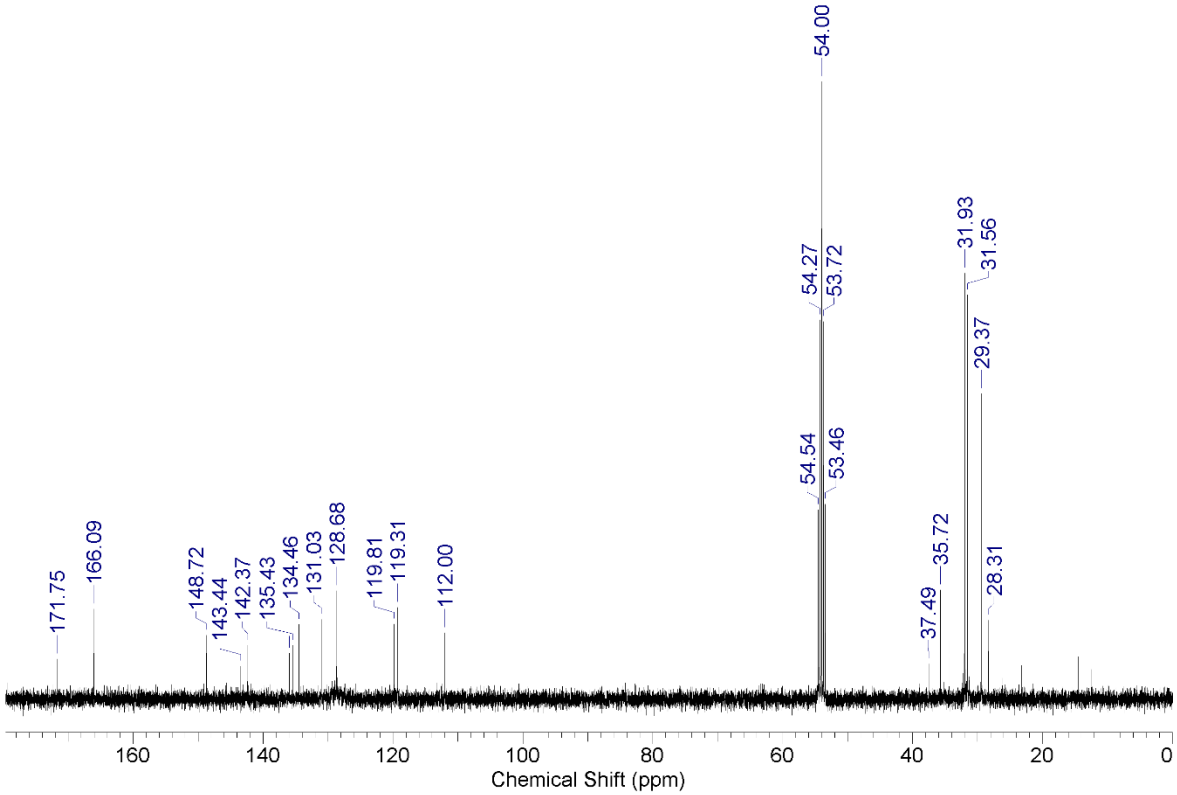

Figure S31. ^{13}C NMR of **6** (CD_2Cl_2, 100 MHz).

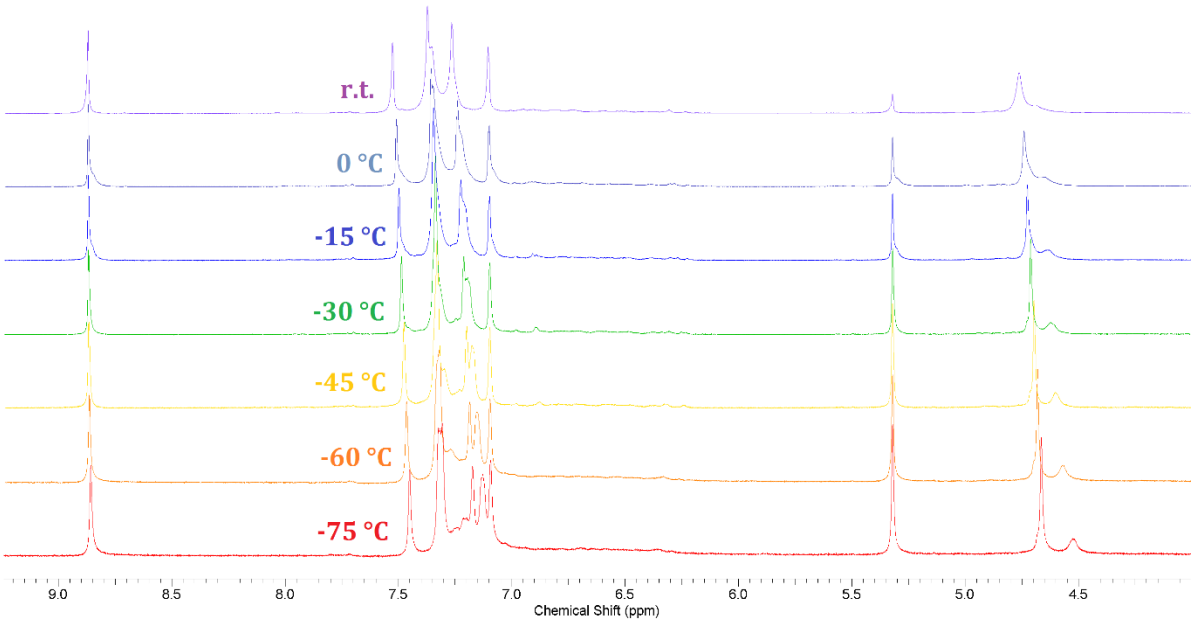

Figure S32. ^{1}H NMR of **6** (CD_2Cl_2, 400 MHz) – low temperature VT studies.

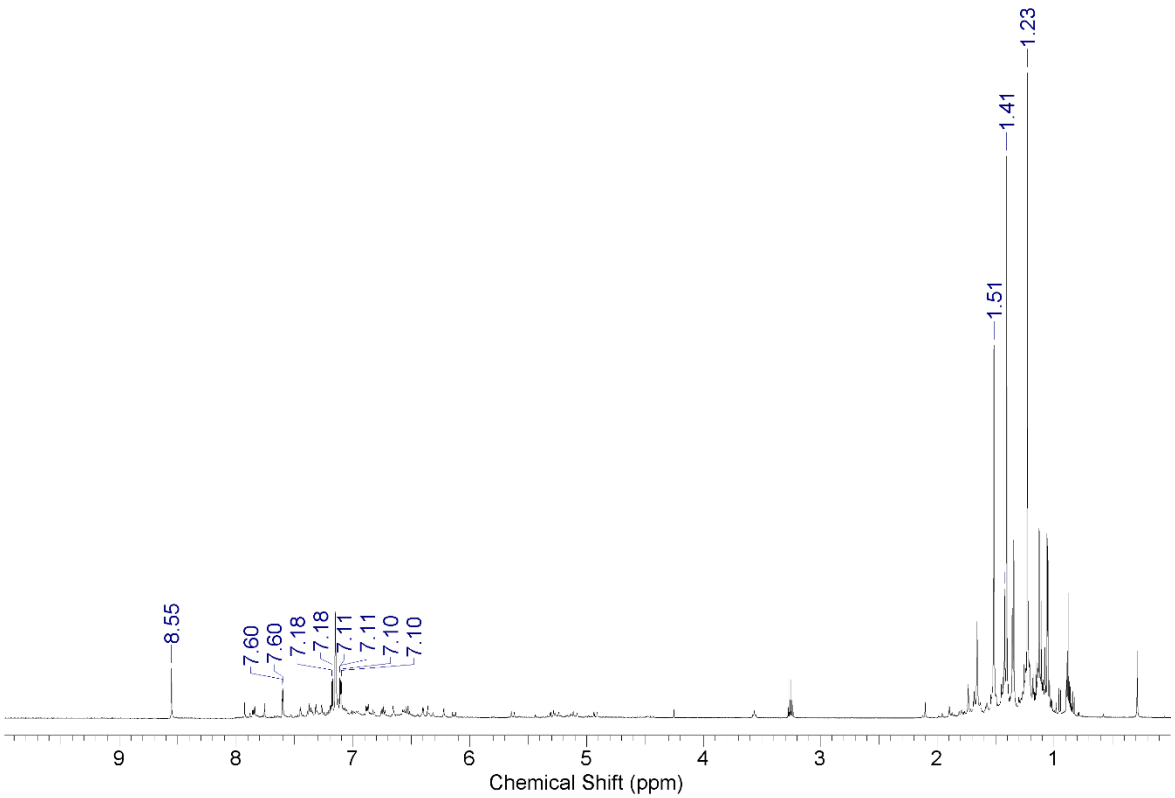

Figure S33. ^{1}H NMR of Decomposition of **6** (C_6D_6, 400 MHz).

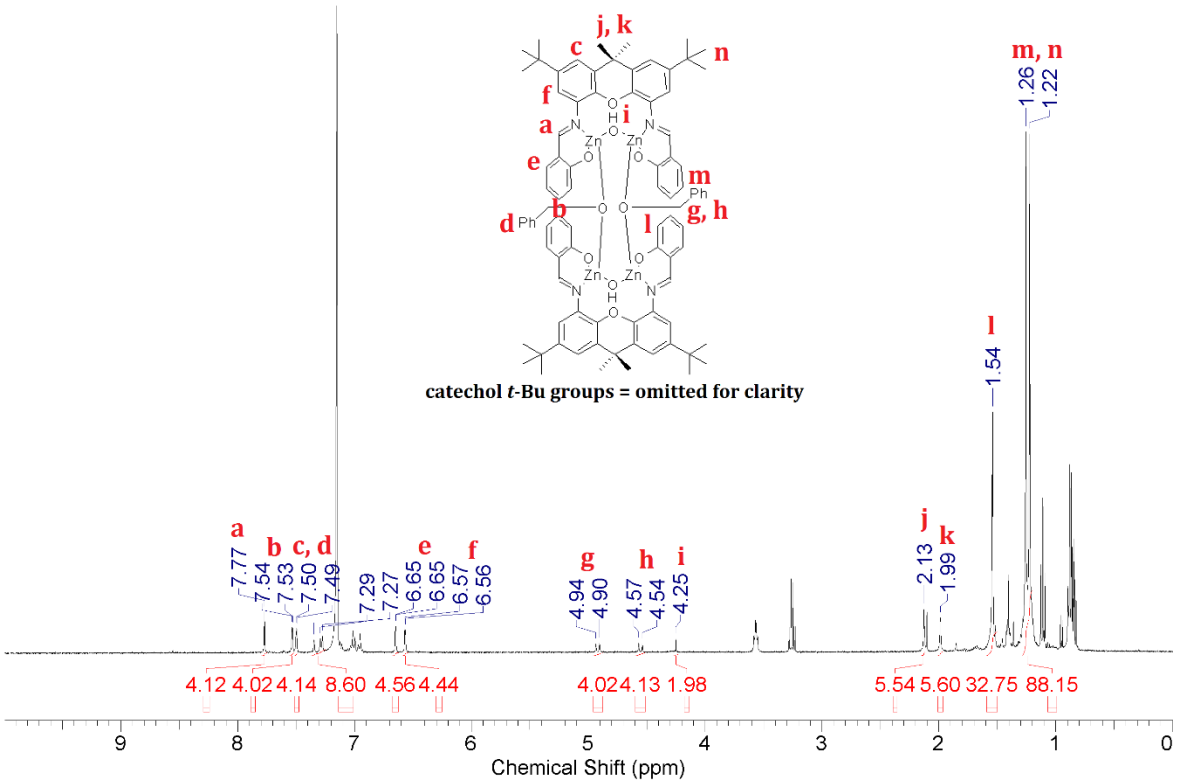

Figure S34. ^{1}H NMR of **7** (C_6D_6, 400 MHz).

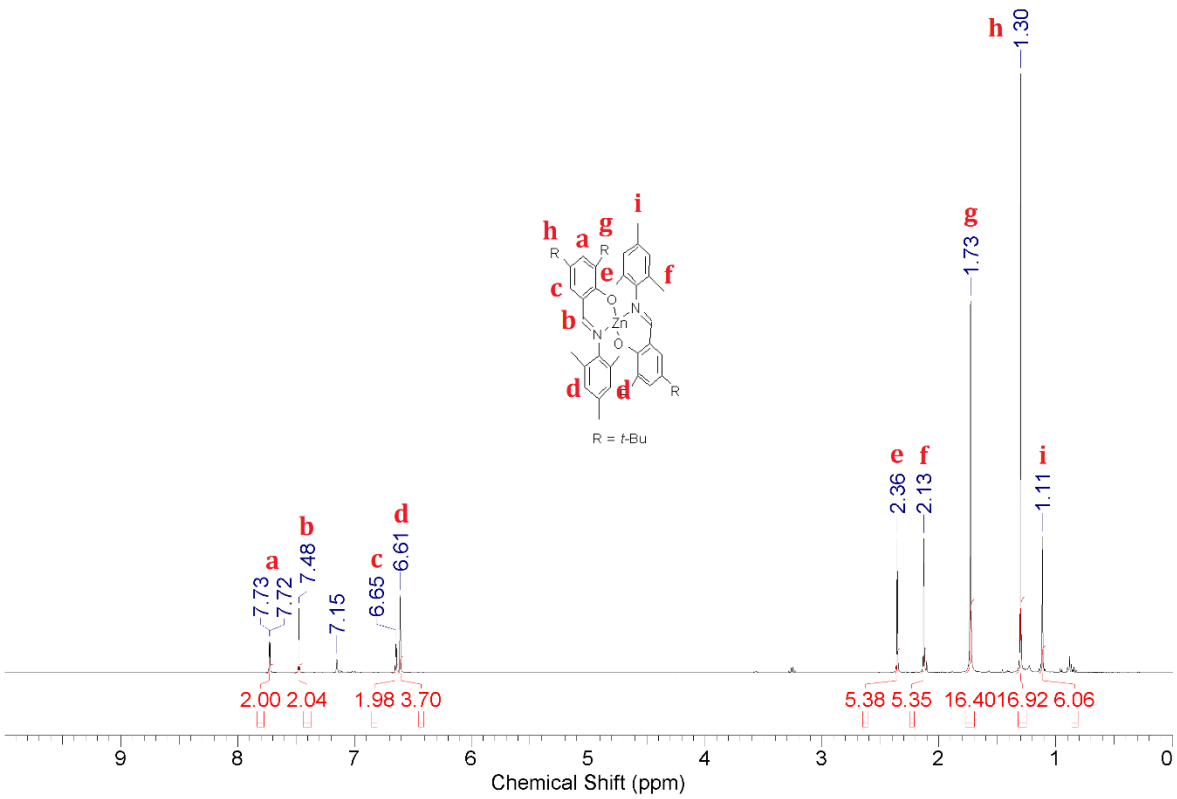

Figure S35. ^{1}H NMR of **8** (C_6D_6, 400 MHz).

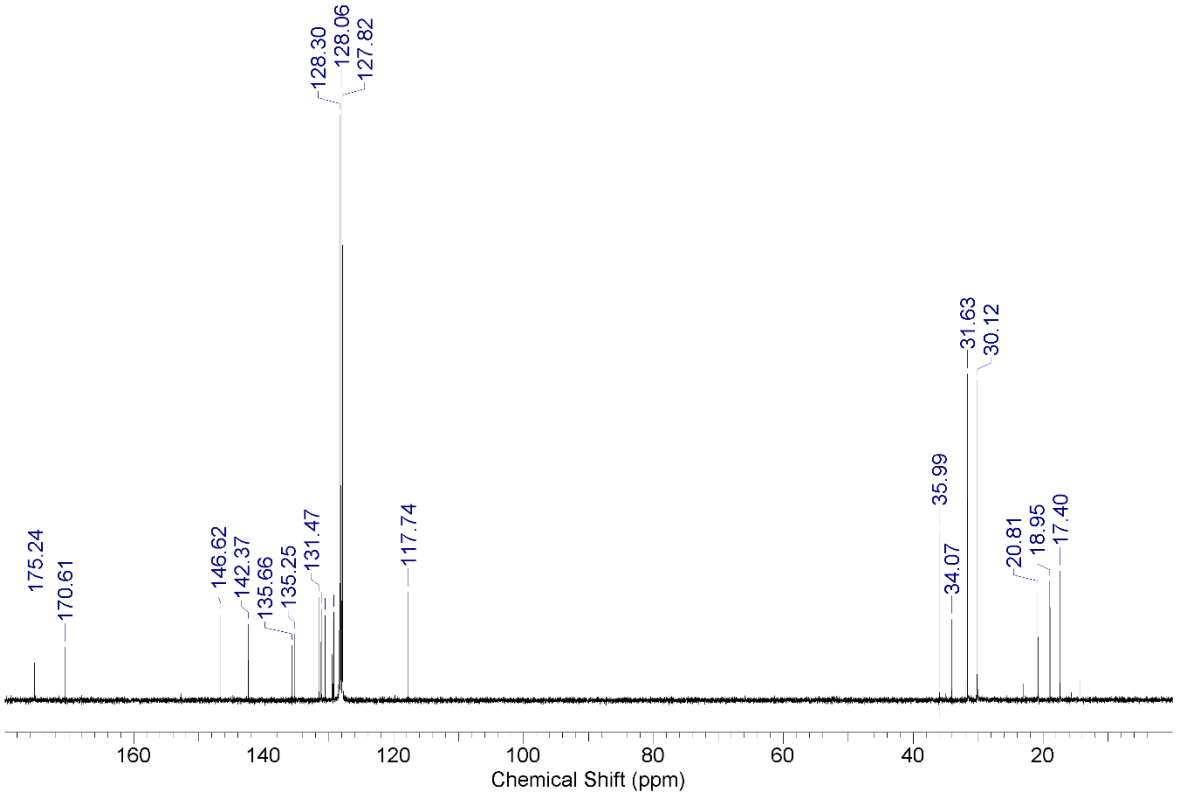

Figure S36. ^{13}C NMR of **8** (C_6D_6, 100 MHz).

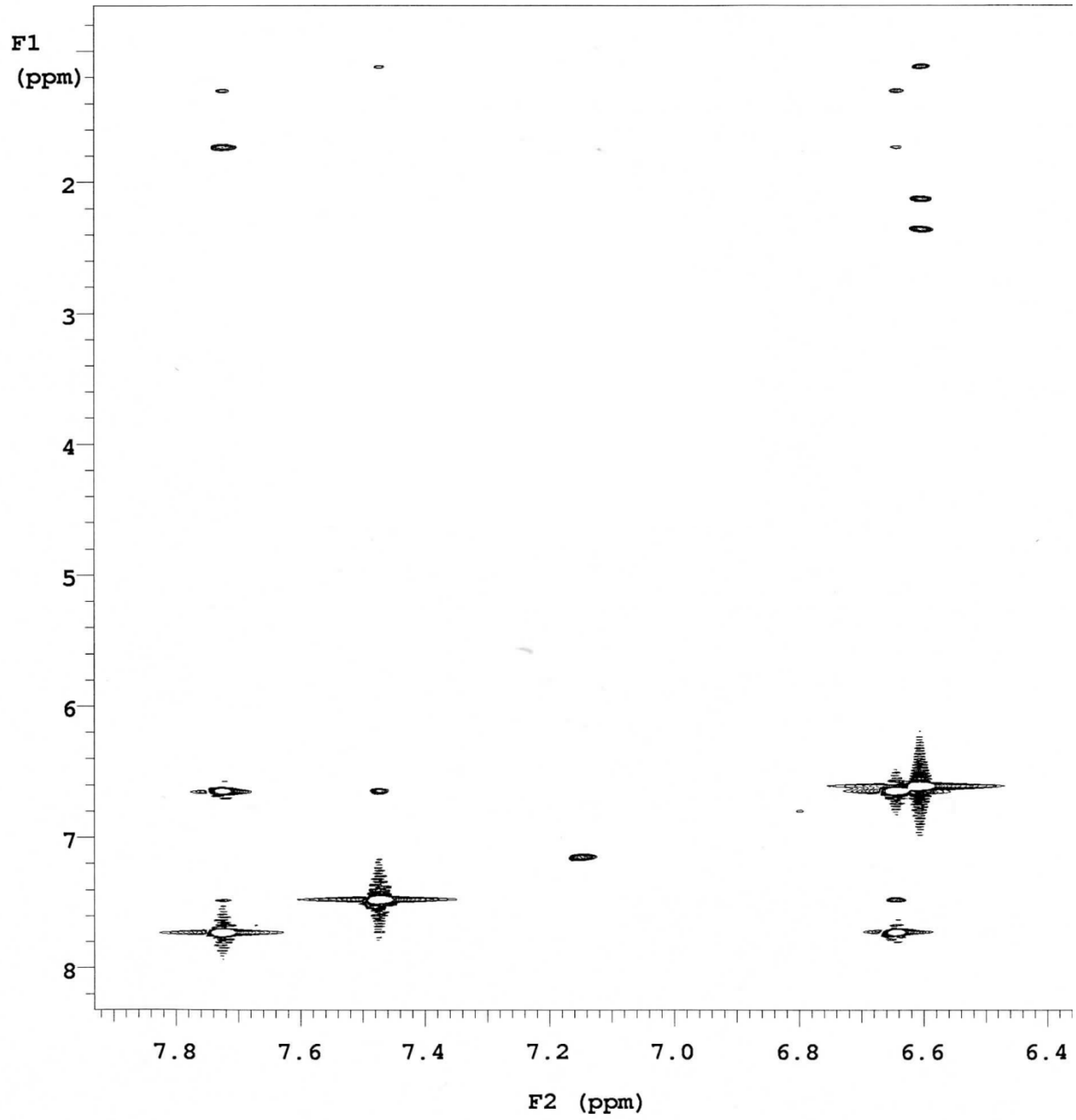

Figure S37. TOCSY NMR of **8** (C_6D_6, 400 MHz) – Aromatic/Aliphatic.

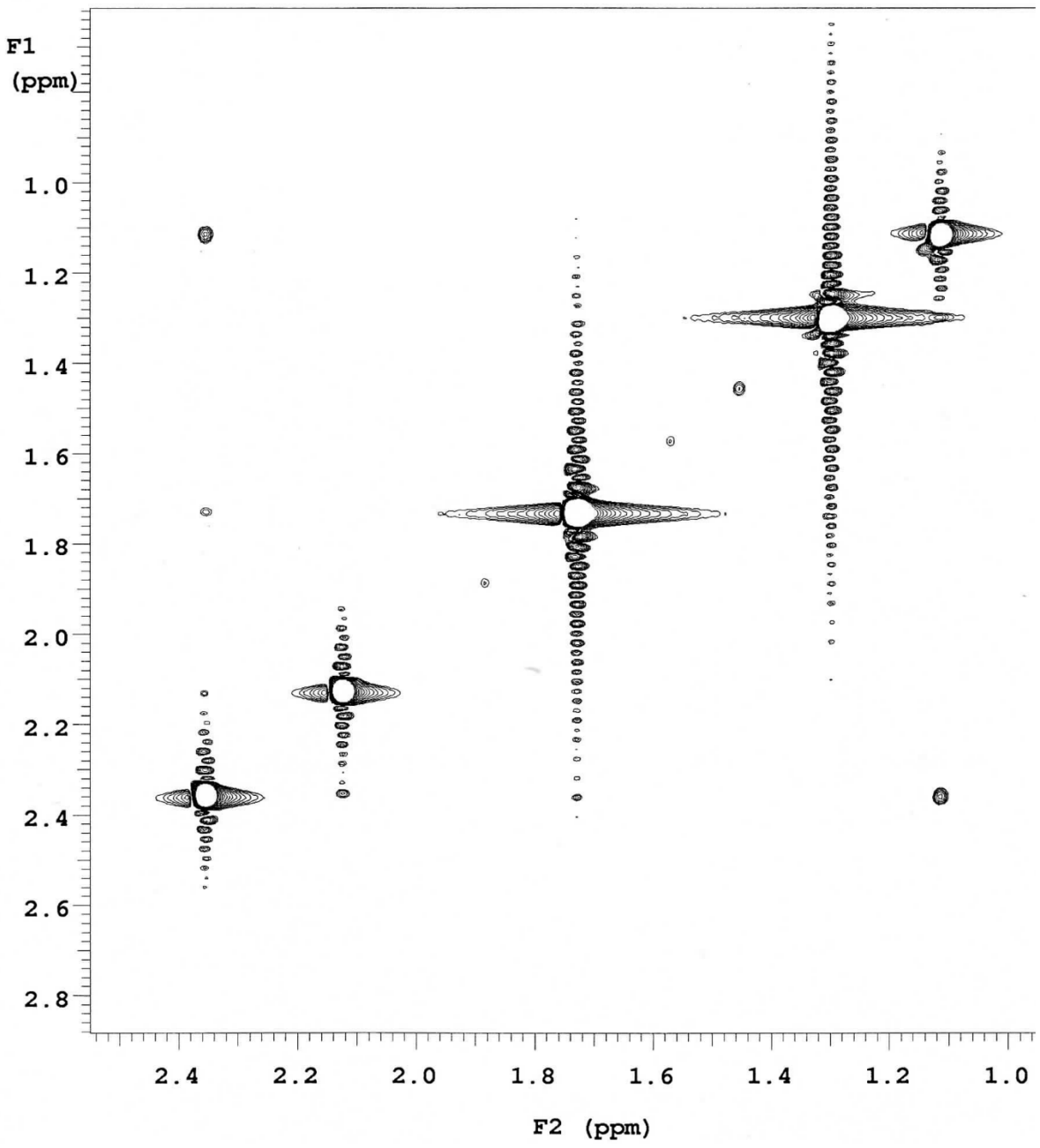

Figure S38. TOCSY NMR of **8** (C_6D_6, 400 MHz) – Aliphatic Region.

4. HD ^{1}H NMR Spectrum of PLA sample

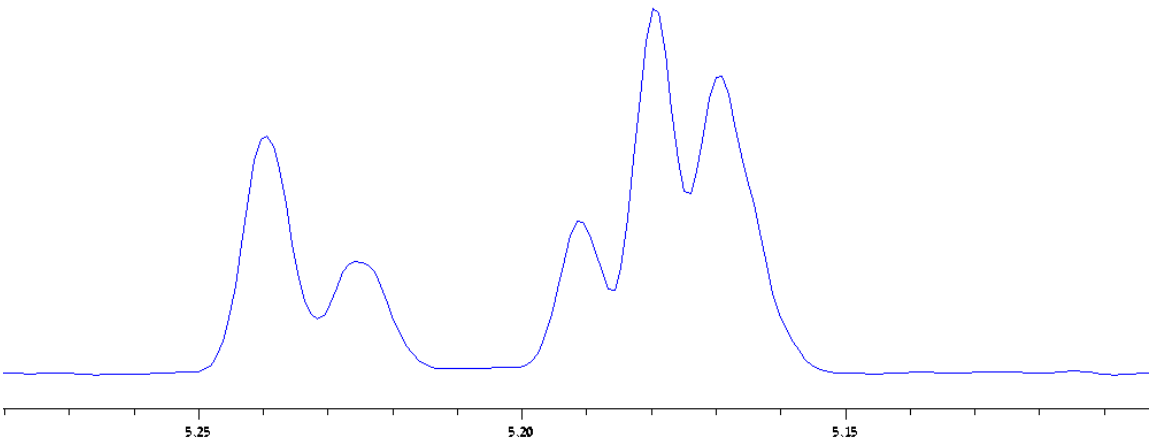

Figure S39. HD ^{1}H NMR (CDCl3, 500 MHz) of heterotactically-inclined PLA (P_r=0.66) prepared with **6** at room temperature.